Langmuir monolayers of cerebroside originated from *Linckia laevigata*: Binary systems of cerebrosides and phospholipid

Tomoki Maruta[a], Kazuki Hoda[a], Masanori Inagaki[b], Ryuichi Higuchi[b], Osamu Shibata[a,*]

[a] *Division of Biointerfacial Science, Graduate School of Pharmaceutical Sciences, Kyushu University,*
3-1-1 Maidashi, Higashi-ku, Fukuoka 812-8582, Japan
[b] *Division of Natural Products Chemistry, Graduate School of Pharmaceutical Sciences, Kyushu University,*
3-1-1 Maidashi, Higashi-ku, Fukuoka 812-8582, Japan

Abstract

The surface pressure (π)–area (A), the surface potential (ΔV)–A and the dipole moment ($\mu_\perp$)–A isotherms were obtained for six cerebrosides of LLC-2, LLC-2-1, LLC-2-8, LLC-2-10, LLC-2-12, and LLC-2-15, which were isolated from *Linckia laevigata*, and two-component monolayers of two different cerebrosides (LLC-2 and LLC-2-8) with phospholipid of dipalmitoylphosphatidylcholine (DPPC) on a subphase of 0.15 M sodium chloride solution as a function of cerebroside compositions in the two-component systems by employing the Wilhelmy method, the ionizing electrode method, and the fluorescence microscopy. The new finding was that LLC-2 showed a stable and liquid expanded type film. Four of them (LLC-2-8, -10, -12, and -15) had the phase transition from the liquid-expanded (LE) to the liquid-condensed (LC) states at 298.2 K. The apparent molar quantity changes (Δs^γ, Δh^γ, and Δu^γ) on their phase transition on 0.15 M at 298.2 K were calculated. The miscibility of cerebroside and phospholipid in the two-component monolayers was examined by plotting the variation of the molecular area and the surface potential as a function of the cerebroside molar fraction ($X_\text{cerebroside}$), using the additivity rule. From the A–$X_\text{cerebroside}$ and ΔV_m–$X_\text{phospholipid}$ plots, a partial molecular surface area (PMA) and an apparent partial molecular surface potential (APSP) were determined at the discrete surface pressure. The PMA and APSP with the mole fraction were extensively discussed for the miscible systems. Judging from the two-dimensional phase diagrams, these were found to be one type, a positive azeotropic type; all the cerebrosides were miscible with DPPC. Furthermore, assuming a regular surface mixture, the Joos equation for the analysis of the collapse pressure of two-component monolayers allowed calculation of the interaction parameter (ξ) and the interaction energy ($-\Delta\varepsilon$) between the cerebrosides and DPPC. The miscibility of cerebroside and phospholipid components in the monolayer state was also supported by fluorescence microscopy.
© 2005 Elsevier B.V. All rights reserved.

Keywords: Langmuir monolayer; Glycosphingolipids; Cerebrosides; Two-dimensional phase diagram; Fluorescence microscopy

1. Introduction

Lipid molecules containing sugar groups are called glycosphingolipids. Glycosphingolipids (GSLs) are present in most animal cell plasma membranes and are thought to play a role in a number of cellular functions, including cell recognition [1,2], cell differentiation [3–5], signal transduction [6,7], apoptosis [8], and receptors for virus [9]. They predominantly locate on the outer leaflet of the membrane and may act to protect the membrane from harsh conditions such as a low pH or degradative enzymes [10]. A detailed description of the chemical, structural and functional properties of glycolipids in general can be found in a review article by Maggio [11].

Glycosphingolipids (GSLs) (cerebrosides) are amphiphilic compounds consisting of saccharide and ceramide moieties and are ubiquitous components of the plasma membrane of all eukaryotic cells [12,13]. Recent cell biological studies show that cerebrosides in plasma membranes form clusters, so called as rafts, with cholesterol and are relatively less con-

* Corresponding author. Tel.: +81 92 642 6669; fax: +81 92 642 6669.
E-mail address: shibata@phar.kyushu-u.ac.jp (O. Shibata).
URL: http://kaimen.phar.kyushu-u.ac.jp.

tent of phospholipids than other areas of plasma membrane. Glycosphingolipids (GSLs) could mediate the signal transduction pathway through interaction with these signaling proteins and not only circulate between the plasma membrane and intracellular organs but also move laterally over the exoplasmic membrane. Such migration could be conducted by raft [14,15]. Galactocerebrosides are a major component of the myelin sheath [16–20]. Glycocerebrosides and lactosylceramide are the major extraneural glycosphingolipids [21–24]. GSLs with tri- and tetrasaccharide containing head groups, known as globosides, are found in the erythrocyte membrane [25]. GSLs show heterogeneity not only in their saccharide head group but also in their ceramide moieties. The biological significance of ceramide heterogeneity is still not well understood. However, especially the structure of ceramide for the fatty acid moieties could influence the localization and functions of GSLs on the plasma membrane, possibly by direct interaction with cholesterol, phospholipids, and the transmembrane domains of receptor proteins [26–29]. Unusual structures of GSLs will be revealed in future through further technological innovation. GSLs exist not only in the vertebrate but also in the mollusk [30], the echinoderm [23,24,31–34], the plant [35,36], and so on; for example, GSLs from the starfish (LMC-1 [23], LMC-2 [23], and LLG-3 [34]).

The interfacial behaviors of GSLs are investigated by using several apparatuses for the monolayer [37–42], the bilayer [43], and the liposome [44,45]. Particularly the monolayer is used as the simplest model of biomembrane. The monolayer properties of GSLs are investigated in terms of the π–A isotherm [37–41], the ΔV–A isotherm [37,40,41], the fluorescence microscopy [40], the Brewster angle microscopy [40], and the atomic force microscopy [41,42]. Some researchers systematically investigate the monolayer properties of GSLs by paying much attention to the structure of sugar chain [37–40]. Others investigate multi-component systems, approaching to the biomembrane composition [42].

Especially monogylcosylated ceramides (cerebrosides) are the simplest class of glycosphigolipids; they are important surface molecules found in virtually all cells. Galactosyl ceramides and their metabolites have been shown to possess important functions in promoting the regulation of nerve cell [46], regulating protein kinase C activities [47], and modulating the function of hormone receptors [48]. In the previous studies, we have reported the surface behavior of some pure cerebrosides and of two-component monolayers made from cerebrosides (LMC-1 and LMC-2) and phospholipids (DPPC and DPPE) [49] and steroids (cholesterol and cholesteryl sodium sulfate) [50,51] at the air–water interface. In order to know the detailed interactions of sphingolipids and their roles in the cell membrane, it is necessary to collect more information on their dependence on the molecular structure difference, i.e. the number, location, and orientation of hydroxyl groups attached to the acyl chains. Glycocerebroside is famous for the precursor of gangliosides or the

accumulated substrate of Gaucher disease. Then glycocerebroside has several activities, for example, anti-ulcerogenic activity [52], anti-tumor activity [53], and anti-microbial activity [35]. So, it is expected that glycocerebroside is utilized as a new medical resource from natural products. The monolayer properties of glycocerebroside were reported from 1970s, but all reports used the molecular species of glycocerebroside [37,50,52–61].

Here, we have focused on isolated GSLs from *Linckia laevigata* as new medical natural resources and on characterizing the Langmuir behavior of some pure cerebrosides, phospholipid, and their two-component systems at the air–water interface. Surface pressure (π)–A, surface potential (ΔV)–A, and dipole moment ($\mu_\perp$)–A isotherms were obtained for the pure compounds and their two-component systems. The phase behavior of two-component monolayers was examined in terms of additivity of molecular surface area and of surface potential. Furthermore, it was analyzed employing the partial molecular area (PMA) and the apparent partial molecular surface potential (APSP). The molecular interaction between monolayer components was investigated using the Joos equation [82]. Finally, the monolayers were examined by fluorescence microscopy.

2. Experimental

2.1. Material

The blue sea star *L. laevigata* (Aohitode in Japanese) is belonging to the Ophidiasteridae family, the Phanerozonia order, the Asteroidea class, the Eleutherozoa subphylum, and the Echinodermata phylum of animals. It was collected in the sea near Motobu in Okinawa, Japan in 2000. The chemical structure of isolated cerebrosides (LLC-2, LLC-2-1, LLC-2-8, LLC-2-10, LLC-2-12, and LLC-2-15) from *L. laevigata* used in this study were shown Fig. 1. The more detailed separation and purification were reported elsewhere [62]. All cerebrosides were classified by ^{1}H and ^{13}C NMR spectra, FAB–MS spectra, GC–MS spectra after purification by TLC and HPLC. The compositions of the hydrophobic acyl chain and long chain base (LCB) are given in Table 1.

Table 1
Acyl chain and long chain base (LCB) composition of cerebrosides

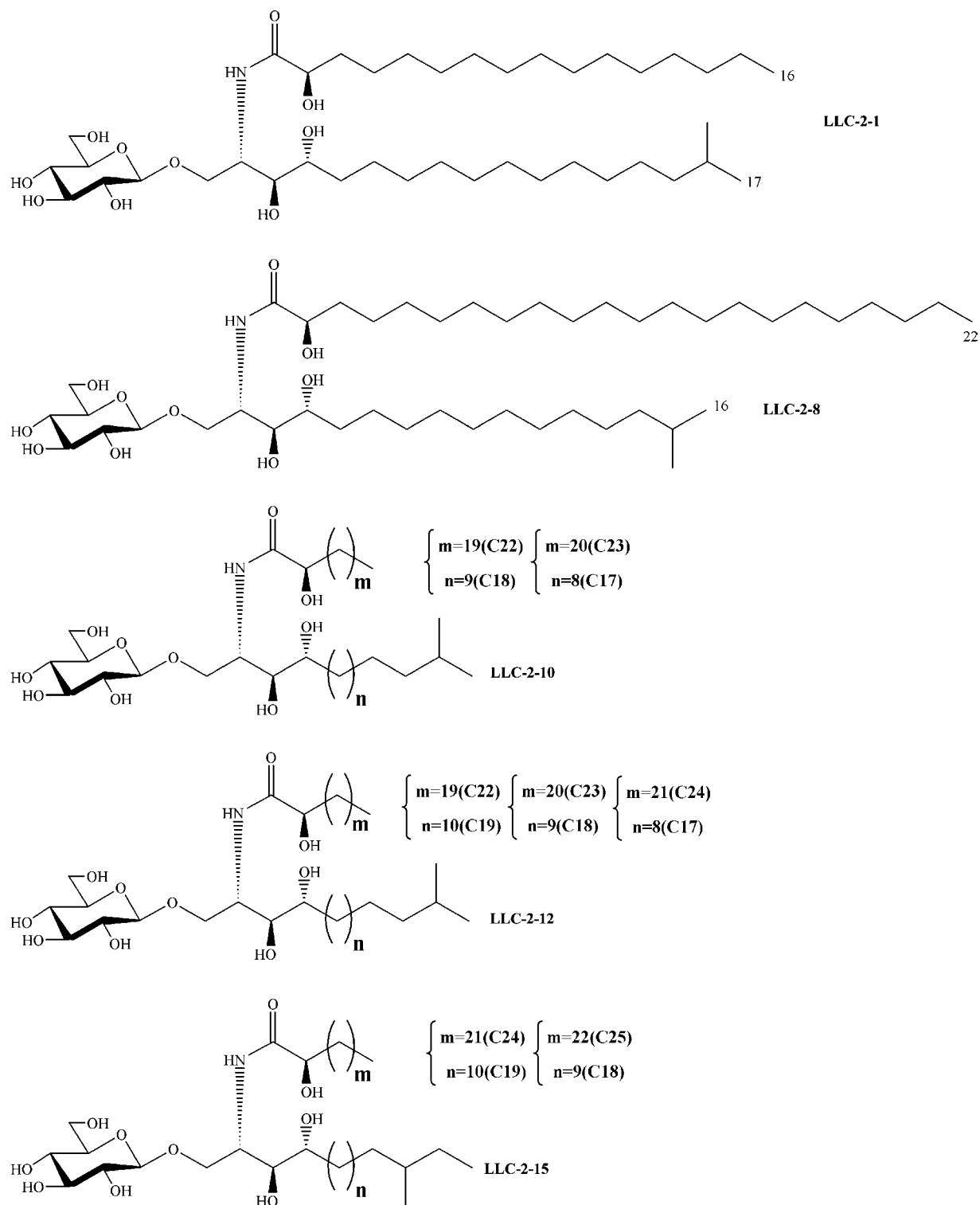|	MW	Fatty acid	LCB	Ratio (%)
LLC-2-1	733	$C_{16:0}$	$C_{18:0}$	100
LLC-2-8	803	$C_{22:0}$	$C_{17:0}$	100
LLC-2-10	817	$C_{22:0}$	$C_{18:0}$	50
		$C_{23:0}$	$C_{17:0}$	50
LLC-2-12	831	$C_{22:0}$	$C_{19:0}$	25
		$C_{23:0}$	$C_{18:0}$	50
		$C_{24:0}$	$C_{17:0}$	25
LLC-2-15	859	$C_{24:0}$	$C_{19:0}$	80
		$C_{25:0}$	$C_{18:0}$	20

Fig. 1. Chemical structures of the cerebroside molecules studied; LLC-2-1, LLC-2-8, LLC-2-10, LLC-2-12, and LLC-2-15. n and m show the carbon number, and parentheses indicate combination of the two chain lengths for the molecular species.

Dipalmitoylphosphatidylcholine (L-α-1-palmitoyl-2-hy-droxy-*sn*-glycero-3-phosphocholine: DPPC) was purchased from Avanti Polar Lipids Inc. (Birmingham, Alabama, USA), the purity was >99% and used without further purification. The pure compounds or their mixtures were spread from the chloroform/methanol mixture (2:1) at the air/aqueous solution interface. Chloroform and methanol were purchased from Cica-Merck (Uvasol). The substrate solution of 0.15 M sodium chloride (Nacalai Tesque) was prepared using thrice distilled water (surface tension, 71.96 mN m^{-1}

at 298.2 ± 0.1 K; resistivity, 18 MΩ cm). Sodium chloride (Nacalai Tesque) was roasted at 1023 K for 24 h to remove any surface active organic impurity.

2.2. π–A and ΔV–A measurements

The surface pressure of the monolayer was measured using an automated home-made Wilhelmy film balance, which was the same as that used in the previous studies [63,64]. The surface pressure balance (Mettler Toledo, AG245) had resolution of 0.01 mN m^{-1}. The surface measuring system was equipped with the filter paper (Whatman 541, periphery 4 cm). The trough was made from aluminum coated with Teflon and its dimension was 500 mm × 150 mm. Before each experiment, the trough was rinsed and cleaned with acetone and chloroform, alternately. The absence of surface-active compounds in the subphase (0.15 M NaCl, about pH 6.5) was checked by reducing the available surface area to less than 4% of its original area after sufficient time was allowed for adsorption of possible impurities that might be present by trace amounts in the substrate. Only substrate that did not show changes of surface pressure above 0.5 mN m^{-1} and of surface potential 50 mV on this procedure was used. A monolayer was mainly prepared by spreading a 100 μL solution at 298.2 K. A period of time, 15 min was needed to evaporate the spreading solvent, and then the monolayer was compressed at the speed of 0.103 nm^2 molecule^{-1} min^{-1}, because no influence of difference in the compression rate (at 0.11 nm^2 molecule^{-1} min^{-1}) could be detected within the limits of the experimental error.

2.3. Fluorescence microscopy

Fluorescence images were observed using an automated home-made Wilhelmy film balance equipped with a fluorescence microscope (BM-1000, U.S.I. System, Japan) [63,64]. It is possible to record simultaneously the surface pressure (π)–area (A) and the surface potential (ΔV)–A isotherms along with the monolayer images to correlate these properties of the same monolayer. A 300 W lamp (XL 300, Pneum) was used for fluorescence excitation. A 546 nm band path filter (Mitutoyo) was used for excitation and a 590 nm cut-off filter (Olympus) for emission. The monolayer was observed using a 20× long-distance objective lens (Mitutoyo $f = 200$/focal length 20 mm). A xanthylium 3,6-bis(diethylamino)-9-(2-octadecyloxycarbonyl)phenyl chloride (R18, Molecular Probes) was used as an insoluble fluorescent probe. It has its absorbance and emission band maxima at 556 and 578 nm, respectively. The solution used in the fluorescence microscopy experiments contained 1 mol% of the fluorescent probe against insoluble materials. Fluorescence images were recorded with a CCD camera (757 JAI ICCD camera, Denmark) connected to the microscope, and transferred directly into computer memory through an online image processor (VAIO PCV-R53, Sony: video capture soft). All the experiments were carried out in a dark room at var-

ious temperatures. The entire optical set-up was placed on an active vibration isolation unit (Model-AY-1812, Visolator, Japan).

3. Results and discussion

3.1. Surface pressure (π)–area (A), surface potential (ΔV)–A, and dipole moment ($\mu_\perp$)–A isotherms of cerebroside monolayers and phospholipid monolayer

The π–A, ΔV–A and $\mu_\perp$–A isotherms of monolayers made from cerebrosides (LLC-2, LLC-2-1, LLC-2-8, LLC-2-10, LLC-2-12, and LLC-2-15) on 0.15 M NaCl solution at 298.2 K were shown in Fig. 2. The molecular species LLC-2 isotherm showed a typical liquid-expanded monolayer behavior, the high compressibility of LLC-2 over the whole surface pressures and the absence of discontinuities in the π–A isotherms. Its extrapolated area was 0.52 nm^2 and the collapse pressure was 47.0 mN m^{-1} (0.39 nm^2), respectively. This result is very close to those previously reported [50], except for minor distinctions caused by dissimilarities in the molecular species composition.

More fractionated cerebrosides (glycosphingolipids: LLC-2-1, LLC-2-8, LLC-2-10, LLC-2-12, and LLC-2-15) showed the transition pressure (π^{eq}) from the liquid-expanded (LE) state to the liquid-condensed (LC) state, whose π–A isotherms in the expanded scale are shown in Fig. 2d. Glycocerebrosides isolated from various species were different in terms of the ceramide core structure, the terminal structure, and the chain length. All cerebrosides employed in this study possess an identical hydrophilic head group. Difference in average molecular areas results from variation in the packing state of the hydrophobic chains with slight olefin and branching chain parts. The long-chain bases (LCB) of LLC-2-1 and LLC-2-8 consist of 16-methyl-heptadecane-1,3,4-triol and 15-methyl-hexadecane-1,3,4-triol chains, respectively, while the LCB of LLC-2-10, LLC-2-12 and LLC-2-15 are mixtures of various chain lengths (Table 1). That is, the LCB of LLC-2-10 consists of 15-methyl-hexadecane-1,3,4-triol (50%) and 16-methyl-heptadecane-1,3,4-triol (50%) chains, while that of LLC-2-12 does 15-methyl-hexadecane-1,3,4-triol (25%), 16-methyl-heptadecane-1,3,4-triol (50%), and 17-methyl-octadecane-1,3,4-triol (25%) and that of LLC-2-15 does 15-methyl-hexadecane-1,3,4-triol (20%), and 16-methyl-octadecane-1,3,4-triol (80%) chains.

The monolayer properties of glycocerebrosides had been reported by using the molecular species [37,49–51,54–58]. A minor component LLC-2-1 in LLC-2 showed more expanded state than LLC-2 in the π–A isotherms at 298.2 K, which was based on its shorter hydrocarbon chain length. The pure compound LLC-2-1 isotherm also showed a typical liquid-expanded (LE) and collapse pressure at 48.8 mN m^{-1} (0.44 nm^2). In contrast, the isotherm of the pure compound of LLC-2-8 showed the characteristic first-order transi-
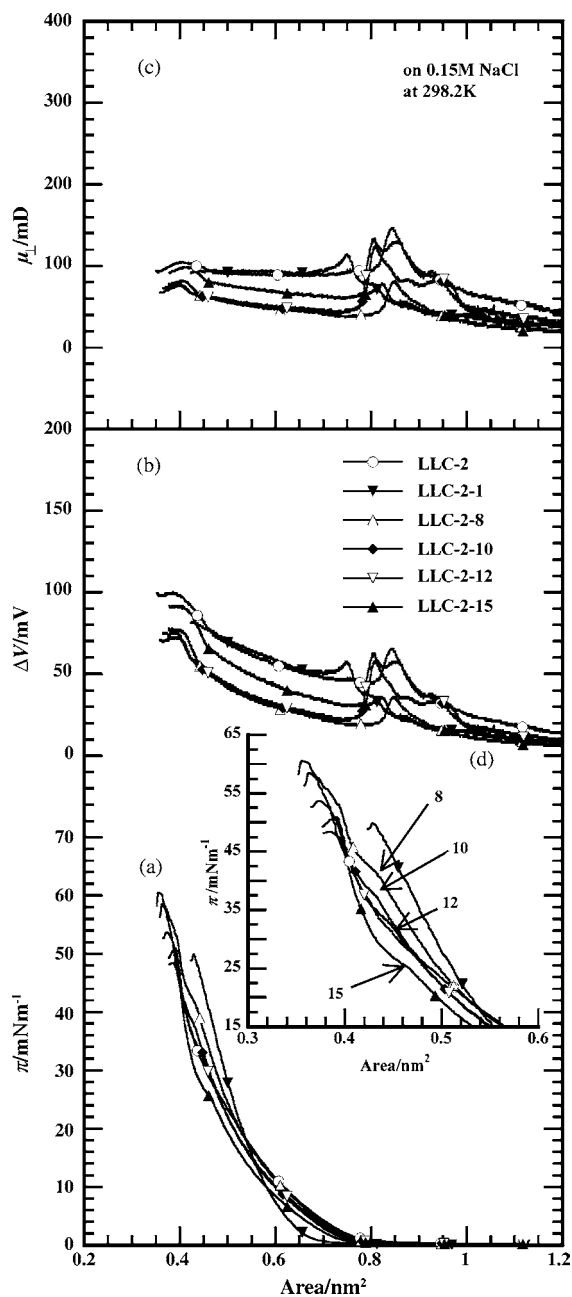
Fig. 2. Surface pressure (π)–area (A) isotherms (a), surface potential (ΔV)–A isotherms (b), surface dipole moment ($\mu_\perp$)–A isotherms (c), and expanded surface pressure (π)–area (A) isotherms (d) of cerebrosides on on 0.15 M NaCl at 298.2 K; LLC-2, LLC-2-1, LLC-2-8, LLC-2-10, LLC-2-12, and LLC-2-15. Arrow shows the transition pressure of each cerebroside.

tion from liquid-expanded (LE) phase to liquid-condensed (LC) phase at 41.2 mN m^{-1} as shown by an arrow number 8 in Fig. 2d. The LLC-2-8 monolayer collapsed at 49.3 mN m^{-1} (collapsed area: 0.40 nm^2), and the extrapolated area was 0.47 nm^2. Also, LLC-2-10, -12, and -15 have the LE/LC phase transition pressure (π^{eq}) at 37.2, 33.2, and 25.0 mN m^{-1}, and their extrapolated areas were 0.47, 0.46, and 0.46 nm^2, respectively. And also the collapse pressures were 48.0 mN m^{-1} (collapsed area: 0.40 nm^2),

46.3 mN m^{-1} (0.40 nm^2), and 42.6 mN m^{-1} (0.40 nm^2), respectively.

The longer the hydrocarbon chains are, the lower the transition pressure becomes and the smaller the extrapolated area does. These behaviors result from the cohesive hydrophobic interaction. However, in spite of the increasing cohesive force, the collapse pressure became lower in the following order LLC-2-8 > -10 > -12 > -15. It may be due to the steric hindrance at the hydrophobic part packing by the terminal *iso*-type structure. These results seem to suggest the hint that the molecular species like LLC-2 regulate the organism by multi-components (such as LLC-2-1, -8, -10, -12, and -15) in biological systems.

All cerebrosides employed in this study possess an identical hydrophilic head group. Differences of their average molecular areas result from variation in the packing state of the hydrophobic chains of slight olefin and branching chain parts.

To check the packing in the monolayer state, surface potential is useful. The surface potential (ΔV) is a measure of the electrostatic field gradient perpendicular to the surface and thus varies considerably with the molecular surface density. The behaviors of ΔV–A isotherms for cerebrosides correspond to the change of the molecular orientation upon compression as shown in Fig. 2b. The surface potentials (ΔV) of cerebrosides showed always positive. The LLC-2 monolayer showed the largest variation of ΔV under compression among them, which reached a value of around 100 mV at the closest packing state. The LLC-2-8 monolayer showed the smallest ΔV value of 70 mV at high surface pressure.

The vertical component of surface dipole moment, $\mu_\perp$ was calculated from the Helmholtz equation using the measured ΔV values,

$$\Delta V = \frac{\mu_\perp}{\varepsilon_0 \varepsilon A}, \tag{1}$$

where ε_0 is the permittivity of a vacuum and ε the mean permittivity of the monolayer (which is assumed to be unity). A is the area occupied by a molecule. The ΔV values involve the resultant of the dipole moments carried by the polar head (saccharide), the C–H bond (the CH$_3$ group), and the subphase. As the subphase and the hydrophilic head are identical for the present four cerebrosides, the difference observed in the ΔV values for the cerebrosides clearly evidences the magnitude of influence of the hydrophobic tails.

3.2. Surface dipole moments ($\mu_\perp$) of cerebrosides

The surface potential of monolayers was often analyzed using the three-layer model proposed by Demchak and Fort [65], which is based on the earlier model of Davies and Rideal [66]. This model postulates independent contributions of the subphase (layer 1), polar head group (layer 2), and hydrophobic chain (layer 3). Independent dipole moments and effective local dielectric constants are attributed to each of the three layers. Other models, such as the Helmholtz model and the

Vogel and Möbius model are also available [67]. These different models were reviewed [68]. The conclusion was that, despite its limitations, the Demchak and Fort model provides good agreement between the $\mu_\perp$ values estimated from the monolayer surface potentials and those determined from measurements on bulk material for various aliphatic compounds.

The estimation of $\mu_\perp$ (the vertical components of the dipole moment to the plane of the monolayer) of polar head groups and hydrocarbon chains using the Demchak and Fort model assumes a condensed Langmuir monolayer of close-packed vertical chains [65,66]. Application of this model to mainly the cerebrosides LE monolayer may lead to a rough estimation. However, if the value of closest-packed cerebrosides monolayer is applied to this model, it may lead to a useful estimation, which can help to provide qualitative explanation of surface potential behavior.

We have thus compared the experimental values of $\mu_\perp$ in the most condensed state of the monolayer with those calculated $\mu_{\perp calc}$ by the three-layer model-based equation,

$$\mu_{\perp calc} = \frac{\mu_1}{\varepsilon_1} + \frac{\mu_2}{\varepsilon_2} + \frac{\mu_3}{\varepsilon_3} \tag{2}$$

where μ_1/ε_1, μ_2/ε_2, and μ_3/ε_3 are the contributions of the subphase, polar head group, and hydrophobic chain group, respectively.

We want to determine the contribution of the hydrophobic group of cerebroside. Carboxylic and hydroxyl groups have already been determined by the Demchak and Fort model [59]. The saccharide of hydrophilic group was also determined by previous report [49].

The initial set of values proposed by Demchak and Fort ($\mu_1/\varepsilon_1 = 0.040$ D, $\varepsilon_2 = 7.6$, and $\varepsilon_3 = 5.3$ [65]) were determined for monolayers made from terphenyl derivatives and octadecyl nitrile. Another set of values were determined in the papers by Petrov et al. ($\mu_1/\varepsilon_1 = 0.025$ D, $\varepsilon_2 = 7.6$, and $\varepsilon_3 = 4.2$ [69]) for monolayers of *n*-heptanol and 16-bromohexadecanol. We have used a set of values introduced by Taylor and Oliveira ($\mu_1/\varepsilon_1 = -0.065$ D, $\varepsilon_2 = 6.4$, and $\varepsilon_3 = 2.8$) for monolayers of ω-halogenated fatty acids and amines [68].

To determine the set of the parameters of our experimental condition, the selection of parameter values was done using the standard sample of dipalmitoylphosphatidylcholine (DPPC). In the first approximation, we assume that they are constant independent of the nature of the head group so that they may be evaluated from the data on DPPC. These data are listed in the previous paper [49]. The experimental values of surface dipole moment for DPPC used to determine the set of the parameters were as follows:

$$\mu_\perp(DPPC) = \frac{\mu_1}{\varepsilon_1} + \frac{\mu_2^{PC}}{\varepsilon_2} + \frac{\mu_3^{CH_3}}{\varepsilon_3} = 0.62 \, D \tag{3}$$

In the calculation, it was assumed that the C–X dipole of terminal –CH$_2$X moiety (where X is a hydrogen) was inclined at half the tetrahedral angle (i.e. $54°44'$) with respect to the water surface as suggested by Bernett et al. [70] and that the group moments have the values given by Smyth [71]. In addition, it was assumed that the C−H group moment was 0.4 D, the carbon being negatively charged [72]. So, the vertical contribution of terminal methyl group is 0.33 D. The structure of the saccharide for hydrophilic group is little bit different compared with that of the starfish *Luidia maculata* (LMC) which is reported in the previous paper [49]. But all the cerebrosides employed in this study possess an identical hydrophilic head group. If the value of the saccharide of hydrophilic group is identical to that of LMC, it was set to 0.63 D (that is, $\mu_2^{sac} = 0.63$ D) from previous report [49]. Then, it is possible to compare the packing state of hydrophobic part of each cerebroside in this study. The authors have used the combination of the set of values ($\mu_1/\varepsilon_1 = -0.025$ D, $\varepsilon_2 = 7.6$, and $\varepsilon_3 = 2.8$), because they provide a good agreement between calculated values and experimental values of dipole moments measured on a saline phase.

Secondly, we evaluated the contribution of the hydrophobic tail group of cerebrosides by using the following equation:

$$\mu_\perp(LLC-2-8) = \frac{\mu_1}{\varepsilon_1} + \frac{\mu_2^{sac}}{\varepsilon_2} + \frac{\mu_3}{\varepsilon_3} = 0.075 \, D \tag{4}$$

We assumed here that the contribution of two hydrophobic tails of LLC-2-8 depends on either the two terminal *iso* or *anti-iso* methyl groups and one vertical of C−H bond. So, we used 0.63 D for μ_2^{sac} and inserted this value to Eq. (4), and the contribution of the hydrophobic group became −0.033 D. Then, we can get $\mu_3 = -0.092$. The same procedure was done for other systems. From the above equations, we obtained $\mu_3^{LLC-2} = -0.011$ D, $\mu_3^{LLC-2-1} = -0.039$ D, $\mu_3^{LLC-2-8} = -0.092$ D, $\mu_3^{LLC-2-10} = -0.090$ D, $\mu_3^{LLC-2-12} = -0.076$ D, and $\mu_3^{LLC-2-15} = -0.028$ D. The results were given in Table 2.

As is clear from the values of column μ_3 (D) in Table 2, vector of all cerebrosides in hydrophobic part are negative, which means that the direction of vector tend from air to subphase. This is an opposite direction compared with normal one. This results from structure difference in hydrophilic part between LMC and LLC; the former has three hydroxyl groups, while later has only one. The magnitude of deformation for hydrophobic part for LLC-2-8 and LLC-2-10 is the largest in all the cerebrosides. It comes from the difference in

Table 2
Surface potential data used for dipole moment evaluation

	Area (nm^2)	π (mN m^{-1})	ΔV (mV)	$\mu_\perp$ (D)	μ_3 (D)
LLC-2	0.41	42	97	0.104	−0.011
LLC-2-1	0.46	42	78	0.094	−0.039
LLC-2-8	0.41	47	70	0.075	−0.092
LLC-2-10	0.41	43	71	0.076	−0.090
LLC-2-12	0.41	41	75	0.081	−0.076
LLC-2-15	0.42	35	89	0.098	−0.028

Area is the molecular surface area obtained by the close-packed high-pressure portion of the π–A isotherms, and ΔV is obtained at that point. $\mu_\perp$ is total dipole moment and μ_3 is that of the part for ω-group.

hydrocarbon chain length between fatty acid and long-chain base (LCB) parts. Even though hydrophobic part includes either the two terminal *iso* or *anti-iso* methyl groups and one vertical of C−H bond, LLC-2-15 showed good alignment in all the present cerebrosides. We also discuss the packing density in the later Section 3.4.

3.3. Compression isotherms of cerebrosides/phospholipid two-component monolayers

Next, turning to the discussion toward two-component systems, two combinations of two-component monolayer systems composed of the two cerebrosides (LLC-2 and LLC-2-8) and one phospholipid (DPPC) have been studied in order to clarify the effect of molecular structure, the interaction between two components, and the miscibility on the monolayer state. For the above purpose, the π–A, ΔV–A, and $\mu_\perp$–A isotherms were measured at various compositions at 298.2 K on a 0.15 M NaCl subphase for pure system of LLC-2, LLC-2-8 and DPPC in Fig. 3 and for LLC-2/and LLC-2-8/DPPC two-component systems in Fig. 4A and B, respectively. The isotherms of two-components at discrete mole fractions are also inserted in the corresponding figures. All the curves of the two-component systems sit between those of the respective pure components, and they successively change with the increasing mole fraction of cerebroside.

The π–A, ΔV–A and $\mu_\perp$–A isotherms of monolayers made from DPPC, LLC-2, and LLC-2-8 on 0.15 M NaCl solution at 298.2 K were shown in Fig. 3. The π–A isotherm of DPPC presented the characteristic first order transition from the disordered liquid-expanded (LE) phase to the ordered liquid-condensed (LC) phase (Fig. 3). The transition pressure, π^{eq} at 298.2 K was 11.5 mN m^{-1}, above which the surface pressure rose due to the orientational change. Collapse of the DPPC monolayer occurred at 54.6 mN m^{-1} (0.39 nm^2), and the extrapolated area was 0.46 nm^2.

The ΔV–A isotherms of cerebrosides (LLC-2 and LLC-2-8) and DPPC were shown in Fig. 3b. Absolute surface potential (ΔV) of the cerebrosides showed almost same value of 70–100 mV. Both of them showed a hump in the ΔV–A isotherms, as observed in the previous one [49–51]. This hump comes from the conformational change for cerebroside in the monolayer state. This change may be due to the phase transition from gaseous phase to LE phase, which was observed as the morphological change by using the fluorescence microscopy. The positive and the negative changes in ΔV for this hump indicate that two hydrocarbon chains and the polar head group performed the conformational change. The LE/LC phase transition was clearly reflected on the π–A isotherm, which corresponded to a change in slope on the ΔV–A isotherm. On the other hand, the ΔV–A isotherm of DPPC showed that ΔV was almost constant ($\sim$0 mV) down to a critical area ($\sim$1 nm^2), and steeply increased up to 300 mV. The ΔV variation was always kept positive and eventually reached 550 mV. The steep increase of ΔV reflected conformational change in the monolayer state.
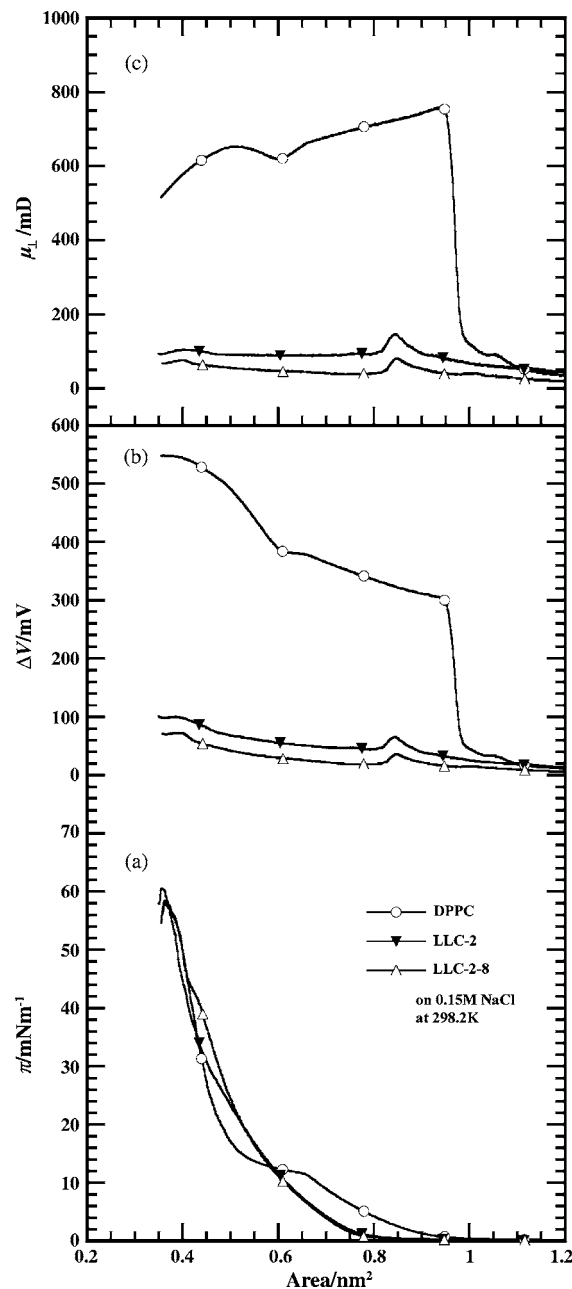

Fig. 3. Surface pressure (π)–area (A) isotherms, surface potential (ΔV)–A isotherms, and surface dipole moment ($\mu_\perp$)–A isotherms of the pure systems on 0.15 M NaCl at 298.2 K; DPPC, LLC-2 and LLC-2-8 systems.

Both the π–A, and the ΔV–A isotherms of DPPC monolayer at subphase of dilute NaCl solutions are very close to those previously reported [64,67–69], except for minor distinctions caused by dissimilarities in subphase composition and temperature.

In spite of having two hydrocarbon chains, absolute surface potential (ΔV) of the cerebrosides was much lower than that of DPPC. It may come from the fact that the packing of hydrophobic part is not very tight due to the terminal *iso*-type structure and/or the hydrophilic part contribution is not so large. All of the cerebrosides indicated almost same ten-
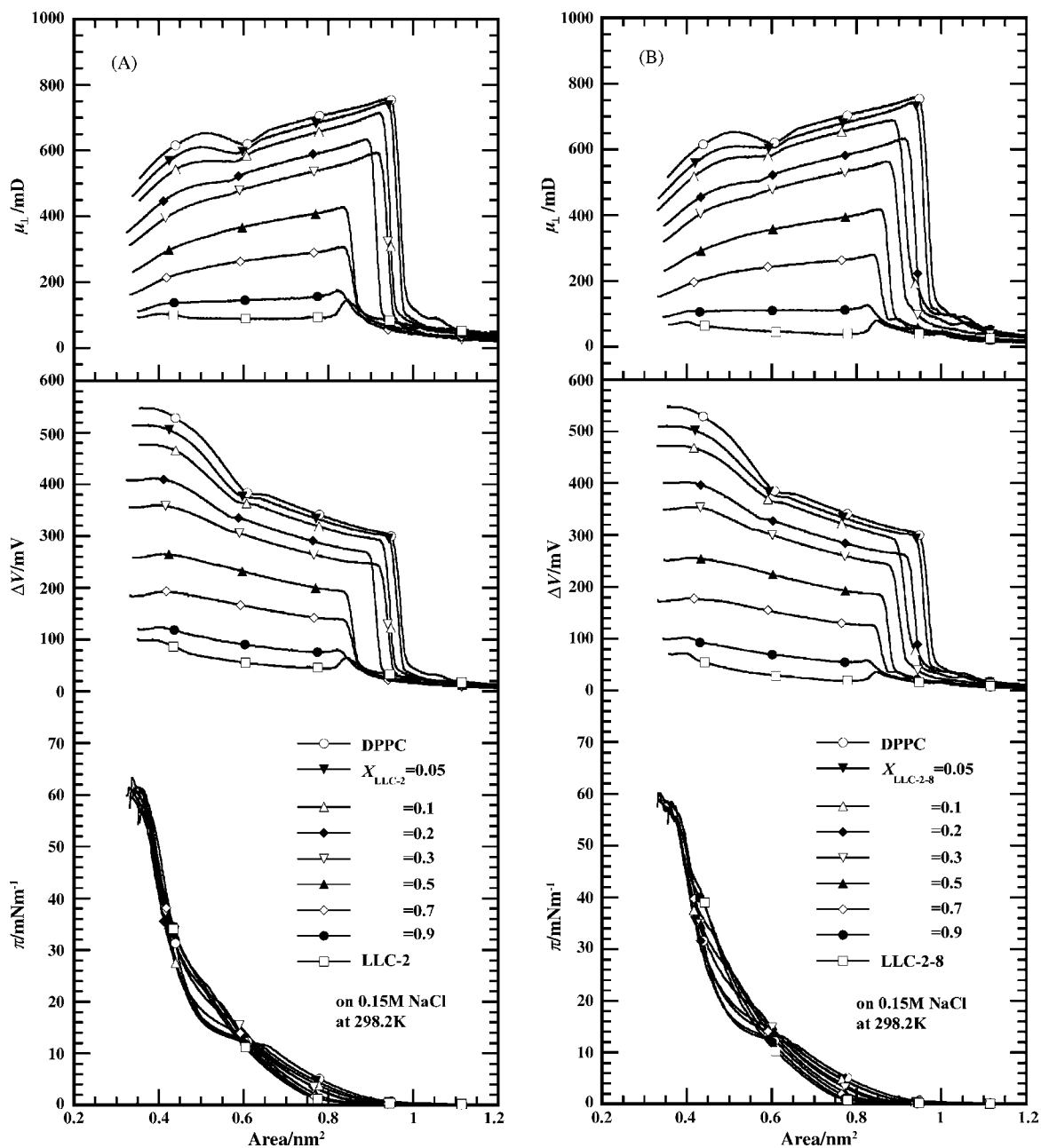
Fig. 4. Surface pressure (π)–area (A) isotherms, surface potential (ΔV)–A isotherms, and surface dipole moment ($\mu_\perp$)–A isotherms of the two-component systems on 0.15 M NaCl at 298.2 K: (A) LLC-2/DPPC and (B) LLC-2-8/DPPC systems.

dency for surface potential behaviors. On the other hand, the $\mu_\perp$–A isotherm of DPPC showed a big change reflected by conformational change in the monolayer state (Fig. 3c).

The π–A isotherms of monolayers for the cerebrosides (LLC-2 and LLC-2–8)/DPPC systems are shown in Fig. 4A and B. Increasing amounts of the DPPC leads to a clearly distinguishable phase transition from liquid-expanded to liquid-condensed phase. The change and appearance of such transition pressure (π^{eq}) with the amount of the cerebrosides suggest that the cerebrosides have an ability to make DPPC miscible in the monolayers, which is mentioned in the later section of two-dimensional phase diagram. This observation

is the first evidence of miscibility for the two components within the monolayer as shown in Fig. 5. As it is difficult to ascertain the presence of the transition pressure at the mole fractions <0.7 on the π–A isotherms, we have investigated cerebrosides/phospholipids (two-component) monolayers by fluorescence microscopy (later section). For $X_{\text{LLC-2}}$ lower than 0.7, the π–A isotherms (Fig. 4A) displayed a phase transition pressure (π^{eq}) that was almost linear against $X_{\text{LLC-2}}$ (Fig. 5A-a). On the other hand, for the whole range of $X_{\text{LLC-2–8}}$, the π–A isotherms (Fig. 4B) displayed a phase transition pressure (π^{eq}) that was almost linear against $X_{\text{LLC-2-8}}$ (Fig. 5B-a). At $X_{\text{LLC-2-8}} = 0.9$, the π–A isotherm showed the
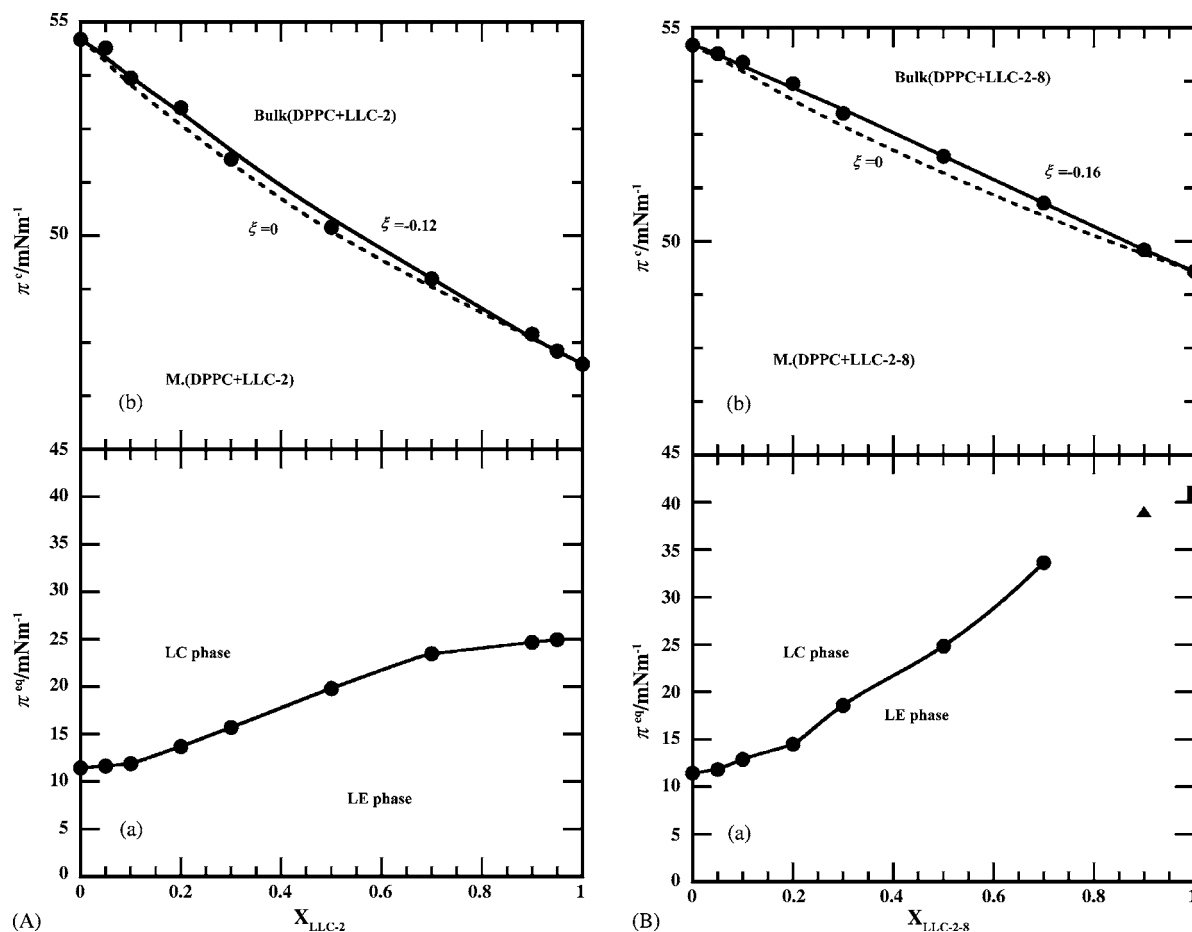
Fig. 5. Change of the transition pressure (π^{eq}) and collapse pressure (π^c) as a function of $X_{cerebroside}$ on 0.15 M NaCl at 298.2 K. The dashed line was calculated by Eq. (10) for $\xi = 0$: (A) DPPC/LLC-2 and (B) DPPC/LLC-2-8 systems.

phase transition, but the fluorescence images did not show the black LC domain like pure LLC-2-8 (mentioned later). So, this transition did not determine which comes from DPPC constituent or LLC-2-8 one. As the result, the two systems of LLC-2/DPPC and LLC-2-8/DPPC showed the miscibility, but there is no clear difference between them.

The interaction between LLC-2 or LLC-2-8 and DPPC molecules was investigated by examining whether the variation of the mean molecular surface areas as a function of $X_{cerebroside}$ satisfies the additivity rule [73,74]. Comparison between the experimental mean molecular areas and the mean molecular areas based on ideal mixing is shown in Fig. 6A and B at five different surface pressures (5, 15, 25, 35 and 45 mN m^{-1}). At $\pi = 5$ mN m^{-1} for LLC-2/DPPC system (Fig. 6A), experimental values show a small negative deviation from the theoretical line, indicating attractive interaction between LLC-2 and DPPC. This may result from the fact that the interactions between LLC-2 and DPPC are mainly governed by the enhanced attractions between hydrophobic groups. At $\pi = 15$ and 25 mN m^{-1} for LLC-2/DPPC system, positive deviations are observed, indicating diminished interaction between the head groups of LLC-2 and DPPC and

between fatty acid chains of LLC-2 and DPPC. At 35 and 45 mN m^{-1}, the variation almost obeys the additivity rule. This indicates that LLC-2 and DPPC are almost ideally mixed in the monolayer. As LLC-2 has a longer alkyl chain than DPPC, attractive interaction between LLC-2 hydrocarbon segments and DPPC chains is maximized and compensates for steric hinderance produced by the LLC-2 hydrocarbon segment. For LLC-2-8/DPPC system (Fig. 6B), comparison of the experimental data with calculated values clearly indicates a good agreement at 5, 35 and 45 mN m^{-1}. The $A–X_{cerebroside}$ shows positive deviations at 15 and 25 mN m^{-1}. These behaviors are explained by the same reason for the LLC-2/DPPC system.

The influence of X_{DPPC} on the $\Delta V–A$ isotherms is shown in Fig. 4A and B. Analysis of the surface potential (ΔV) of the two-component monolayers in terms of the additivity rule is presented in Fig. 7A and B. For LLC-2/DPPC system (Fig. 7A), and the comparison of the experimental data with calculated ones clearly indicates a negative deviation from the ideal line at 15–45 mN m^{-1} and a positive one at 5 mN m^{-1}. Such trend is the same as that for the LLC-2-8/DPPC system (Fig. 7B), too.
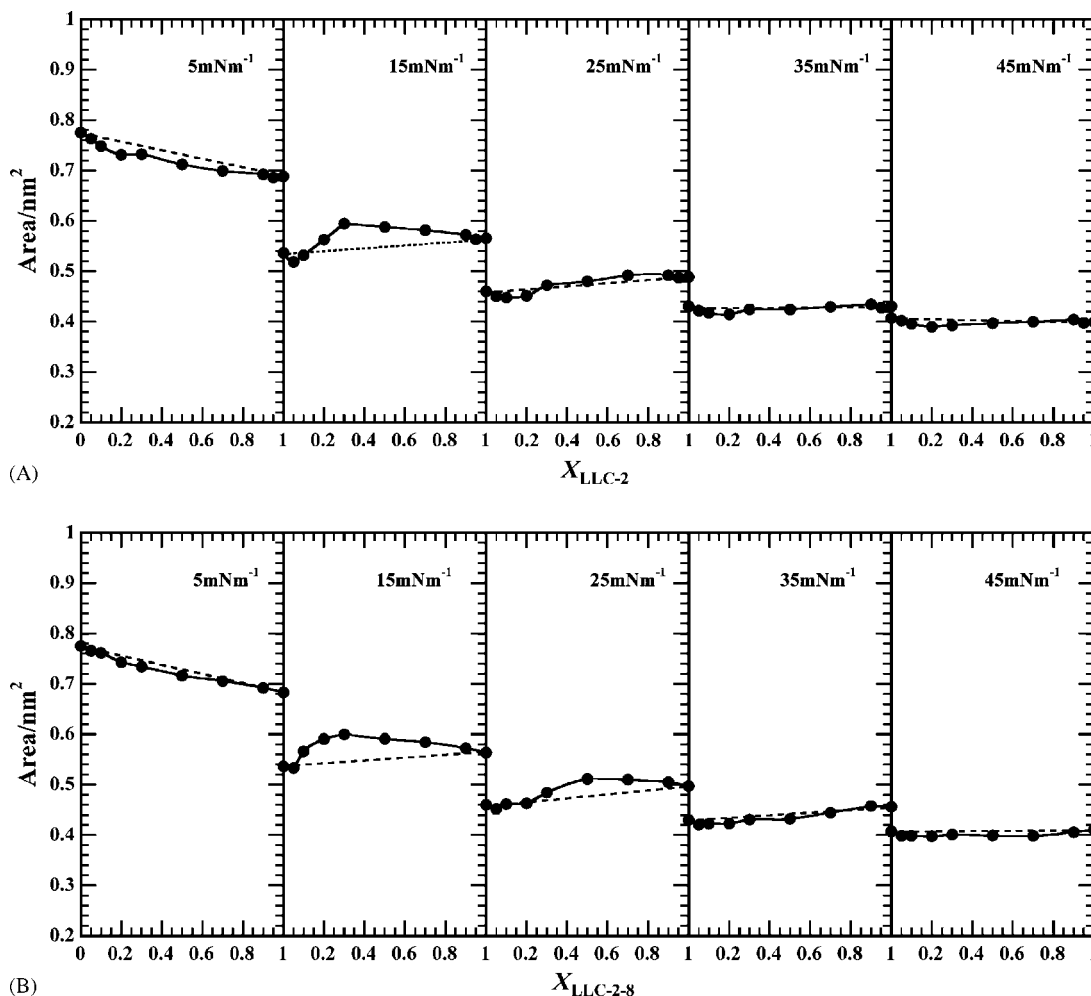
Fig. 6. Deviation of two-component monolayer from ideal behavior. Variation of the mean surface area (A_m) with cereboroside mole fraction for the cerebrosides/phospholipid mixtures at different surface pressures: (A) LLC-2/DPPC and (B) LLC-2-8/DPPC systems.

3.4. Mean molecular surface area (A_m), partial molecular surface area (PMA), mean molecular surface potential (ΔV_m), and apparent partial molecular surface potential (APSP)

When π–A isotherms of a given binary mixture are analyzed, it is essential to examine whether the relation of mean molecular surface area (A_m) with mole fraction (X) satisfies the additivity rule or not and, if not, which deviation is observed, negative or positive. Comparison between experimental mean molecular areas and mean molecular areas calculated for ideal mixing at five surface pressures (5, 15, 25, 35, and 45 mN m^{-1}) was showed in Fig. 6A (LLC-2) and Fig. 6B (LLC-2-8). A binary system can show an ideal behavior either by forming ideally mixed monolayer or by the case where the two components cannot mix at all but can form the so-called patched film, where the additivity should show a linear relation as indicated by a broken line. Here, A_m is assumed to satisfy the following equations:

$$A_m = X_1 A_1 + X_2 A_2 \tag{5}$$

where A_m is the average molecular area in the two-component film, X_1 and X_2 are the mole fractions of the components 1 and 2, respectively, and A_1 and A_2 are the partial molecular areas in the two-component film at a definite surface pressure.

The behaviors of occupied surface area and surface potential can be seen more clearly if the partial molar quantities are evaluated. One of them has been employed in previous study [49,51,75]. When PMA is denoted as A_1 and A_2 for components 1 and 2, the A_1 and A_2 values can be determinable as the respective intercept value at $X_2 = 0$ and $X_2 = 1$ of a tangential line drawn at any given point on the A_m–$X_{\text{cerebroside}}$ curve as shown in Fig. 6. A_1 and A_2 from the relation are given as:

$$A_1 = A_m - X_2 \left(\frac{\partial A_m}{\partial X_2} \right)_{T,\pi}$$
$$A_2 = A_m + (1 - X_2) \left(\frac{\partial A_m}{\partial X_2} \right)_{T,\pi} \tag{6}$$

where A_i is defined as:

$$A_i = \left(\frac{\partial A_t}{\partial N_i} \right)_{T,\pi}$$
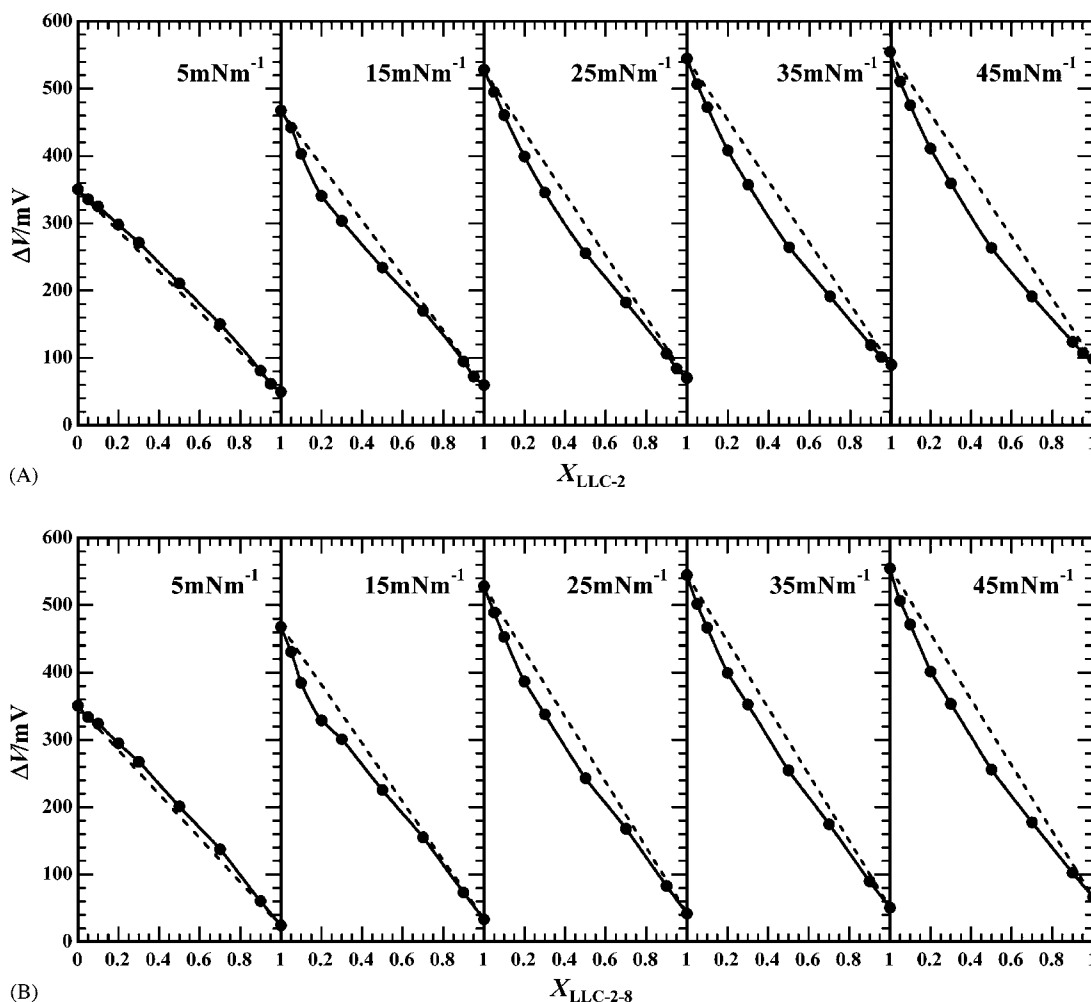
Fig. 7. Deviation of two-component monolayer from ideal behavior. Variation of the surface potential (ΔV) with cereboroside mole fraction for the cerebrosides/phospholipid mixtures at different surface pressures: (A) LLC-2/DPPC and (B) LLC-2-8/DPPC systems.

when N_1 plus N_2 molecules form a surface area A_t ($= N_1 A_1 + N_2 A_2$), and 1 and 2 denote cerebrosides and DPPC, respectively. Correspondingly, the apparent partial molecular surface potential can be obtained from the relationship between the average molecular surface potential and mole fraction, which is the same as the above area.

$$\Delta V_1 = \Delta V_m - X_2 \left(\frac{\partial \Delta V_m}{\partial X_2} \right)_{T,\pi} \qquad (7)$$

where ΔV_m was evaluated by dividing the measured surface potential (ΔV) by the number of molecules in the unit area. The surface potential (ΔV) is measured by an americium air electrode whose area is ca. 1 cm². Therefore, we assumed its dimension to be mV cm^{-2}. The average molecular surface potential in mV molecule^{-1} unit can be obtained by the ΔV and the number of molecules in 1 cm² calculated from the π–A isotherm. When APSP is denoted as ΔV_1 and ΔV_2 for components 1 and 2, they are determined by the respective intercepts at $X_2 = 0$ and $X_2 = 1$ of a tangential line drawn at any given point on the ΔV_m–$X_{cerebroside}$ curve as shown in Fig. 8.

For cerebrosides/DPPC systems, they were miscible due to the evidence of change of transition pressure which increased with $X_{cerebroside}$ (above-mentioned). So, the procedures for PMA and APSP were applied to cerebrosides/DPPC systems. The PMA–$X_{cerebroside}$ curves for cerebrosides (LLC-2 and LLC-2-8)/DPPC systems are shown in Fig. 9. It is noted that if the two-component systems are ideal mixing, the PMA and APSP should be parallel to the axis of X_2 (the additivity rule). The PMA for both cerebrosides/DPPC systems indicates the similar behavior at each surface pressure. It is found that DPPC molecules have almost the same surface area in the binary LLC-2 and LLC-2-8/DPPC systems at low and high surface pressures except for 15 and 25 mN m^{-1}. At 5 mN m^{-1} of LLC-2/DPPC system, the partial molecular areas of LLC-2 and DPPC do not remain constant over the whole mole fraction. On the contrary, as for LLC-2-8/DPPC system, those of LLC-2 and DPPC show almost individual one over the whole mole fraction. At 15 mN m^{-1} of cerebrosides/DPPC systems, the partial molecular areas of both systems are very changeable, too. This complex behavior comes from the LE/LC transition of DPPC. This characteristic PMA behavior may
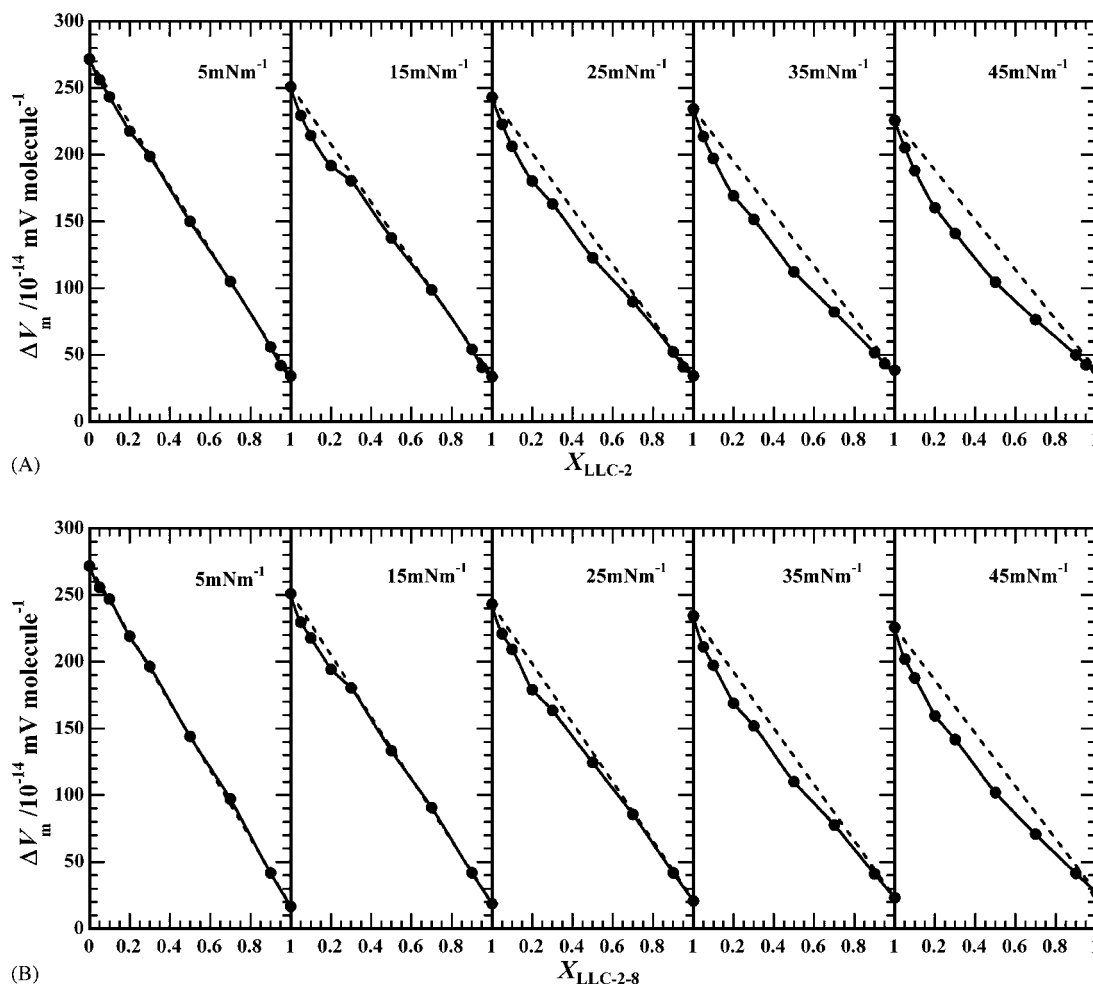
Fig. 8. Variation of the mean molecular surface potential (ΔV_m) with cereboroside mole fraction for the cerebrosides/phospholipid mixtures at different surface pressures: (A) LLC-2/DPPC and (B) LLC-2-8/DPPC systems.

be directly related to the liquid expanded state of DPPC. At the higher surface pressure (35 mN m^{-1}), where DPPC molecules form a liquid condensed film, all molecular areas of the two mixtures show an almost linear in regard to A_m versus X_2 plots, although small deviations from the additivity rule are seen. However, these deviations are not attributable to the experimental errors.

In contrast to PMA, the APSP–$X_{cerebroside}$ curves for cerebrosides/DPPC systems (see Fig. 10) suggest almost same interaction of DPPC between LLC-2 and LLC-2-8. The APSP–$X_{cerebroside}$ for cerebroside/DPPC systems indicates the similar behavior at each surface pressure. It is found that APSP of DPPC and LLC-2 (or LLC-2-8) molecules remain almost the same as the individual value over the whole mole fraction range at low surface pressure (at 5 and 15 mN m^{-1}) as shown in Fig. 10A and B. Upon compression at 35 and 45 mN m^{-1}, APSP of DPPC increases with increasing mole fraction of DPPC. For example, DPPC molecules at $X_{cerebroside} = 0.9$ are surrounded almost by the LLC-2 or LLC-2-8 molecules for the binary LLC-2/DPPC and LLC-2-8/DPPC system. In the monolayer, DPPC has a minimum

molecular area of about 0.46 nm^2 (Fig. 3) [76,77], which is limited by the relatively large head group cross-sectional area. The cross-sectional area of an optimally packed, all trans, hydrocarbon chain is about 0.20 nm^2 [78], so the hydrocarbon portion of the DPPC molecule would like to occupy an area of $A = 2 \times 20$ nm^2 = 0.40 nm^2. This mismatch results in a tilt angle of aliphatic chains of 25–30° and a reduction in the attractive interactions between the chains [75,79]. Tilting is also accompanied by a decrease in the coherence length of monolayer packing.

Addition of LLC-2 (or LLC-2-8) reduces the head/tail mismatch of pure DPPC as shown by potential increase of APSP for DPPC, indicating the decrease in tilt angle of the mixed monolayer state. Upon compression at 25 mN m^{-1}, for the mole fraction of 0.1 and 0.3, part of DPPC changes to LC film via transition pressure π^{eq}. APSP for DPPC indicates the decrease in tilt angle of the mixed monolayer state at the sacrifice of orientation for LLC-2 (or LLC-2-8). Upon compression at 35 mN m^{-1}, APSP of DPPC decreases and that of LLC-2 increases, increasing mole fraction of cerebroside. At the range of $X_{cerebroside} = 0$–0.3, APSP of
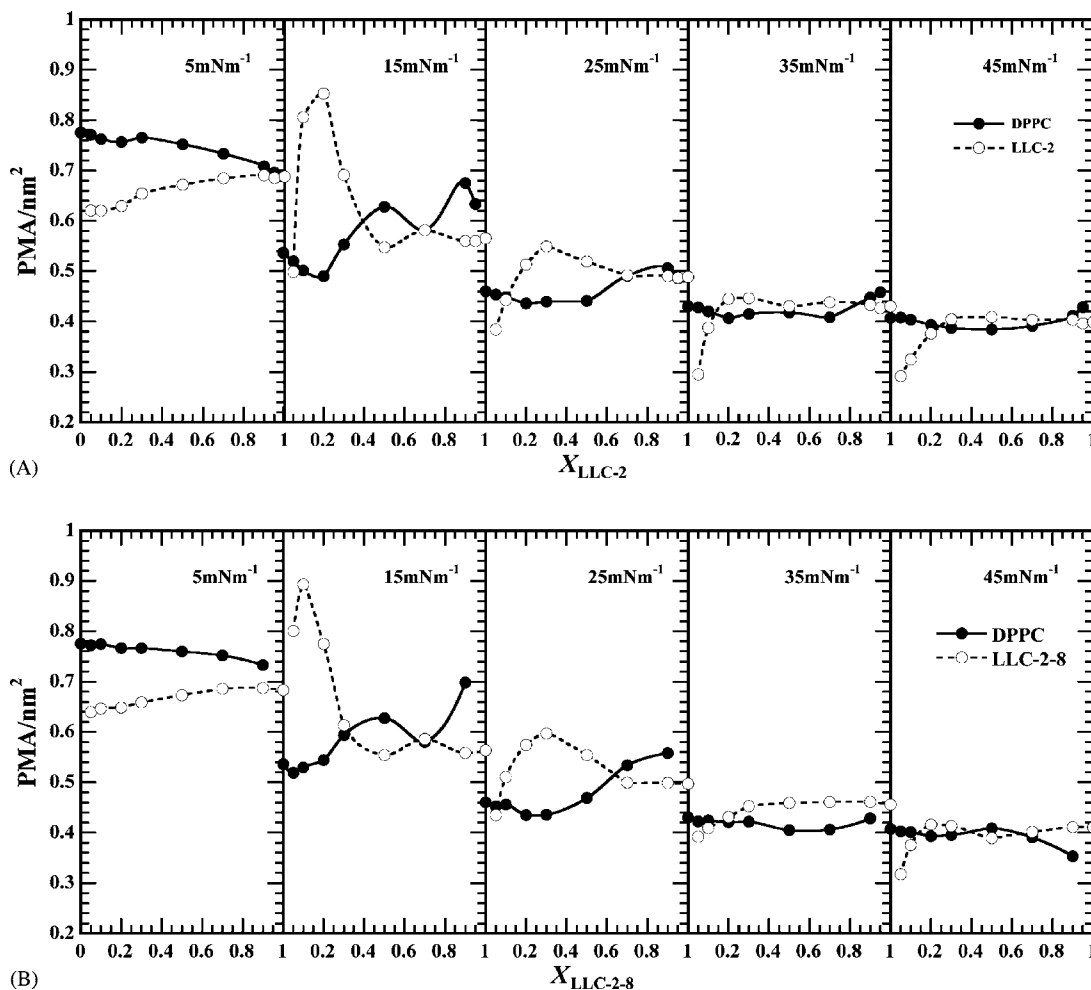
Fig. 9. Variation of partial molecular surface area (PMA) for two-component cerebrosides and DPPC as a function of $X_{\text{cerebroside}}$ at different surface pressures: (A) LLC-2/DPPC and (B) LLC-2-8/DPPC systems.

DPPC remains almost constant, after that, that of DPPC and then decreases above the mole fraction. On the contrary, at the range of $X_{\text{cerebroside}} = 0.05$–$0.5$, APSP of LLC-2 (or LLC-2-8) increases almost linearly and then reaches almost the individual value which increasing cerebroside mole fraction.

The packing for the LLC-2 (or LLC-2-8)/DPPC system changes depending upon the surface pressure. This behavior is owing to the matching of the chain length of DPPC (saturated) and to the position of methyl group (*iso* or *anti-iso*) in LLC-2 (or LLC-2-8) chains (saturated). In consequence, the surface orientation of DPPC molecules is affected more strongly by LLC-2 chains than LLC-2-8 ones due to the mixing of position of methyl group in LLC-2 chains.

3.5. Apparent molar quantity changes on the phase transition

The temperature effect on the phase transition pressure of the monolayer is of much interest, since it provides us with the thermodynamic information on the phase transi-

tion of monolayers. Fig. 11 shows the representative π–A isotherms of LLC-2–15 cerebroside on 0.15 M NaCl solution at various temperatures. Similar isotherms were observed for LLC-2-1, LLC-2-8, LLC-2-10, and LLC-2-12 systems. All the curves have a break point, showing the phase transition from LE phase to LC phase on compression. This phase transition was also confirmed by surface potential and fluorescence microscopy. As was expected, the transition pressures increased with increasing temperature. The isotherm of LLC-2-1 did not show the LE/LC phase transition at 298.2 K but showed the transition below 293.2 K in Fig. 12. The π–A isotherm showed that the collapse pressure decreased with increasing temperature. For example, the collapse pressures of LLC-2-8 were 54.0, 51.4, and 49.3 mN m^{-1} at 288.2, 293.2, and 298.2 K, respectively (figure not shown). In addition, they showed that the variation of surface potential (ΔV) roughly tended to decrease with increasing temperature. For example, the variation of surface potential of LLC-2-8 was 83, 78, and 70 mV at 288.2, 293.2, and 298.2 K, respectively. These results are caused by looser packing with increasing temperature.
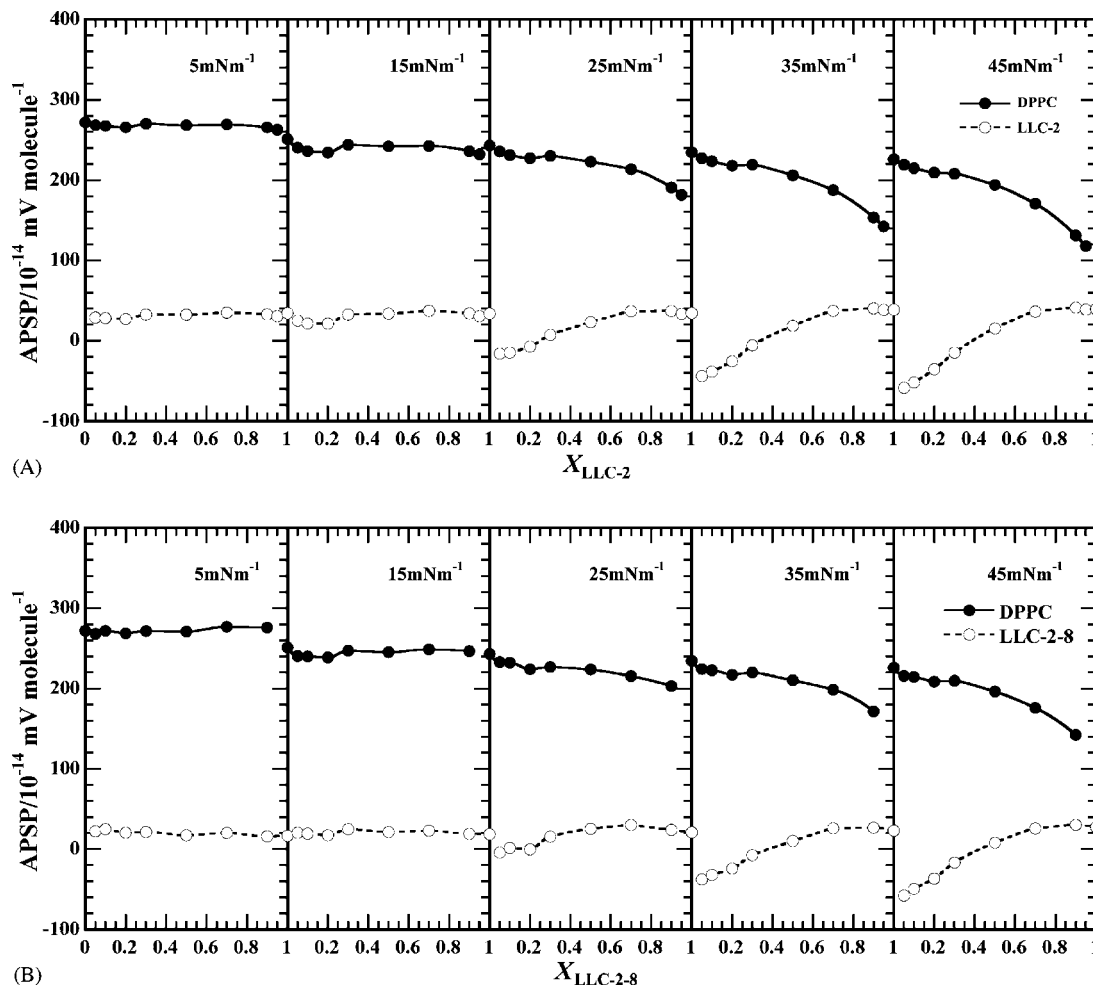
Fig. 10. Variation of apparent partial molecular surface potential (APSP) for two-component cerebrosides and DPPC as a function of $X_{cerebroside}$ at different surface pressures: (A) LLC-2/DPPC and (B) LLC-2-8/DPPC systems.

The temperature dependence of the transition pressure (π^{eq}) for the cerebrosides is shown in Fig. 12. The inclination of LLC-2-1 was quite different from the others. This reason is that the structure of LLC-2-1 is different from others in terms of balance for the hydrocarbon chains between fatty acid and the long-chain base (LCB) parts. The curves are almost linear, and the slopes of these curves were used to calculate the apparent molar quantity change on the phase transition. The change of thermodynamic quantities on the phase transition of monolayer was calculated using the previous method [80,81], which takes the contribution of the substrate of a monolayer into account. The apparent molar entropy change (Δs^γ) on the phase transition was evaluated by the following equation:

$$\Delta s^\gamma(\alpha, \beta) = (a^\beta - a^\alpha)\left[\left(\frac{\partial \pi^{eq}}{\partial T}\right)_p - \left(\frac{\partial \gamma^0}{\partial T}\right)_p\right] \tag{8}$$

In this equation, Δs^γ is an apparent molar entropy change, a^α and a^β are molecular areas (in square nanometers, the superscripts α and β refer phase states), π^{eq} the transition pressure from the β phase to the α phase, and γ^0 the surface

tension of the substrate. a^α and a^β are estimated as follows. a^β is the area at the point where the film starts to transform from the β to the α state. The a^α value is determined in the following manner; when the point (π^{eq}, a^β) is moved parallel to the area axis to zero area, it comes into contact with the elongated line of the π–A isotherm of the S (solid) state to the lower surface pressure. The intersection point gives the a^α value. The right hand side of Eq. (8) is calculated numerically from the π–A isotherms given in Fig. 11. Moreover, the apparent molar enthalpy change (Δh^γ) and the apparent molar energy change (Δu^γ) on the phase transition were related to Δs^γ by

$$\Delta h^\gamma(\alpha, \beta) = T \Delta s^\gamma(\alpha, \beta) \tag{9}$$

$$\Delta u^\gamma(\alpha, \beta) = (\pi^{eq} - \gamma^0)(a^\beta - a^\alpha) + T \Delta s^\gamma(\alpha, \beta) \tag{10}$$

Thus, we can determine Δh^γ and Δu^γ by use of the above experimental results.

The apparent molar quantity changes (Δs^γ, Δh^γ, and Δu^γ) on the first-order phase transition for LLC-2-8, -10, -12, -15 and DPPC on 0.15 M NaCl at 298.2 K are given in Table 3. This table also includes the apparent molar quan-
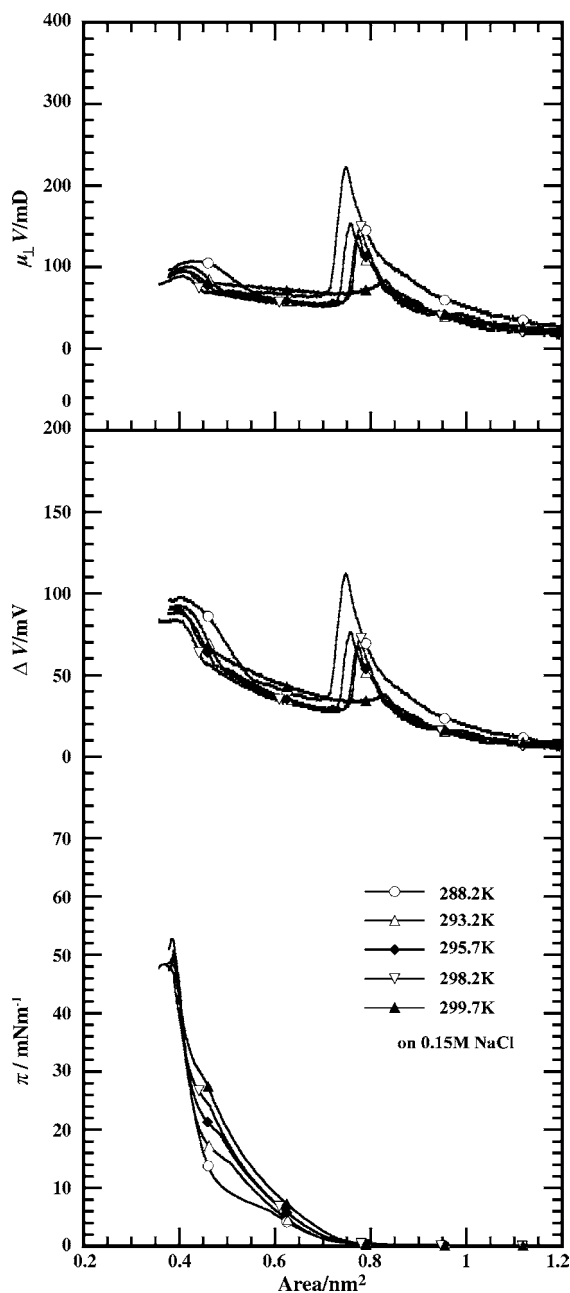
Fig. 11. The temperature dependence of surface pressure (π)–area (A) isotherms, surface potential (ΔV)–A isotherms, and surface dipole moment ($\mu_\perp$)–A isotherms of the one-component system on 0.15 M NaCl at various temperatures for LLC-2-15 system.
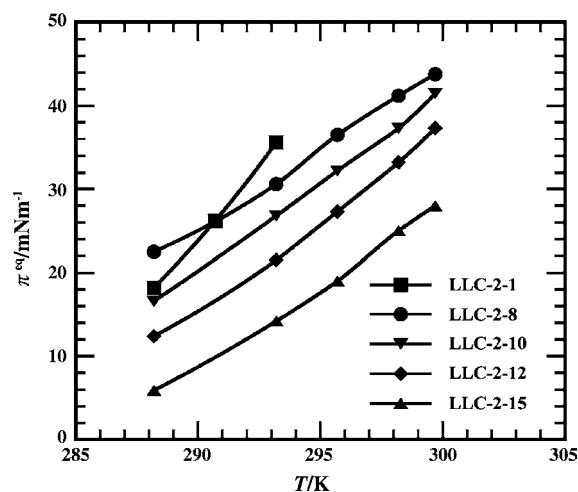

Fig. 12. The transition pressure (π^{eq}) on 0.15 M NaCl at various temperatures for different cerebroside systems.

tity changes of tetradecanoic acid in order to compare with those of cerebrosides. It can be seen from Table 3 that for the apparent molar enthalpy changes, all the values are negative as expected. That is, the transition from the disordered phase (gaseous or expanded) to the ordered one is exothermic.

Let us look at the entropy column in Table 3, where longer the chain length of fatty acid part of cerebrosides are, larger the value of Δs^γ become. The apparent molar quantity changes depended on the chain length combination based on the extent of cohesive force of hydrocarbon chain in cerebrosides. The values of the apparent molar quantity changes on the phase transition for cerebrosides were almost the same as that of the tetradecanoic acid.

However, the apparent molar quantity changes on the phase transition for cerebrosides were lowered by one order of magnitude, compared with that of DPPC. This comes from the difference in hydrophobic part packing between the terminal *iso*-type structure and saturated hydrocarbon chain alignment.

3.6. Two-dimensional phase diagram

From the π–A isotherm for the binary systems of LLC-2/DPPC and LLC-2-8/DPPC, their two-dimensional phase diagrams were constructed by use of the transition pressures (π^{eq}) and/or the collapse pressures (π^c) at various mole fractions of cerebrosides. Representative phase diagrams at 298.2 K are shown in Fig. 5A and B.

The transition pressures from disordered (gaseous- or liquid-expanded) to ordered (liquid-condensed) phase are also plotted against the mole fraction of cerebroside in Fig. 5a. In LLC-2/DPPC and LLC-2-8/DPPC systems, π–A isotherm displays the phase transition pressure (π^{eq}) that changes almost linearly with $X_{cerebroside}$ from 0.05 to 0.7. Judging from the change of the transition pressure, two components at all other mole fractions are miscible each other. This behavior is a first evidence of the miscibility of the two components

Table 3
Apparent molar quantity changes (Δs, Δh, and Δu) for cerebrosides on the phase transition on 0.15 M NaCl at 298.2 K

	$-\Delta s^\gamma$ (JK^{-1} mol^{-1})	$-\Delta h^\gamma$ (kJ mol^{-1})	$-\Delta u^\gamma$ (kJ mol^{-1})
LLC-2-8	38	11	12
LLC-2-10	40	12	13
LLC-2-12	54	16	17
LLC-2-15	70	21	22
DPPC	217	65	72
Myristic acid[80]	47	14	17

in the monolayer state. This can be explained by the fact that the film forming molecules become more dense by compression, leading to decrease in the surface tension more by the film forming molecule. Then the resultant surface pressure increased.

Assuming that in these cerebrosides/DPPC cases the surface mixtures behave as a regular solution with a hexagonal lattice, the coexistence phase boundary between the ordered monolayer phase and the bulk solid phase can be theoretically simulated by the Joos Eq. (11), and the interaction parameter (ξ) was calculated from this deviation [82].

$$x_1^s \gamma_1 \exp\left(\frac{\pi_{c,m} - \pi_{c,1}}{kT}\omega_1\right)\exp\left[\xi(x_2^s)^2\right]$$
$$+ x_2^s \gamma_2 \exp\left(\frac{\pi_{c,m} - \pi_{c,2}}{kT}\omega_2\right)\exp\left[\xi(x_1^s)^2\right] = 1 \qquad (11)$$

where x_1^s and x_2^s denote the mole fraction in the two-component monolayer of components 1 and 2, respectively, and $\pi_{c,1}$ and $\pi_{c,2}$ are the corresponding collapse pressures of components 1 and 2. $\pi_{c,m}$ is the collapse pressure of the two-component monolayer at given composition of x_1^s and x_2^s. ω_1 and ω_2 are the corresponding limiting molecular surface area at the collapse points. γ^1 and γ^2 are the surface activity coefficients at the collapse point, ξ is the interaction parameter, and kT the product of the Boltzmann constant and the Kelvin temperature.

In these figures, M indicates a two-component monolayer formed by cerebroside, and DPPC species, while Bulk denotes a solid phase of cerebrosides and DPPC ("bulk phase" may be called "solid phase"). The collapse pressure π^c determined at each mole fraction is indicated by filled circles, where the dotted line shows the case where the interaction parameter (ξ) is zero.

From this equation, the interaction parameter ξ is obtained, and these mixtures yield $\xi = -1.20$ (for LLC-2/DPPC) and -0.16 (for LLC-2-8/DPPC). This means that there is mutual interaction between two components in the two-component monolayer that is stronger than the mean of the interactions between pure component molecules themselves. As the result, they are completely miscible. The interaction energy $-\Delta\varepsilon$ can be calculated by the following equation:

$$-\Delta\varepsilon = -\frac{\xi RT}{6} \qquad (12)$$

and these values are $50\,\mathrm{J\,mol^{-1}}$ (for LLC-2/DPP) and $66\,\mathrm{J\,mol^{-1}}$ (for LLC-2-8/DPPC). As a result, cerebrosides/DPPC systems are the positive azeotropic type.

The value of the interaction energy of LLC-2-8/DPPC is a bit larger than that of LLC-2/DPPC, but much weaker than that of previous reports [49–51,63,64,75,81].

3.7. Fluorescence images of cerebroside monolayer

In order to make clear the phase behavior of the π–A isotherms, we investigated the monolayers by fluorescence

microscopy, which provides a direct image of the monolayers. A fluorescent dye probe was therefore incorporated into the monolayer and its distribution was monitored by fluorescence micrographs. The contrast is due to difference in dye solubility between disordered (or LE) and ordered phases (or LC). Representative fluorescence micrographs (FMs) of pure LLC-2, LLC-2-8, DPPC, and their two-component monolayers spread on 0.15 M NaCl at 298.2 K are shown in Fig. 13A and B at various surface pressures.

Before examining the effects of a cerebroside on DPPC domain shape, it is necessary to make pure DPPC behavior clear. The π–A isotherm of DPPC is shown in Fig. 3a, where there exists the LE/LC coexistence region. Domain nucleation occurs at the kink in the π–A isotherm (typically at $11.5\,\mathrm{mN\,m^{-1}}$). Initially, the domains appear roughly round in shape: whether the shape is the case in reality or due to limits in the resolution of the microscope is unclear. Indeed, only when they grow, they take their fundamental shape in Fig. 13.

Column DPPC in Fig. 13A and B shows a progression of fluorescence images through the coexistence region for DPPC [83–85]. The numerical value indicates surface pressure in the figures for ordinate and mole fraction of cerebroside for abscissa. The images indicate the gaseous phase at $5\,\mathrm{mN\,m^{-1}}$ and the coexistence state of both LE phase and LC phase at 11.5 and $15\,\mathrm{mN\,m^{-1}}$, where the bright regions and dark domains indicate LE and LC phase, respectively. With increasing surface pressure from 11.5 to $15\,\mathrm{mN\,m^{-1}}$, the percentage of LC phase in each image increases and complete LC domain image appears at $20\,\mathrm{mN\,m^{-1}}$ (data not shown). The domains formed are chiral, which is an expression of the chirality of the DPPC molecule. As would be expected, the enantiomer forms mirror images of the domains, and a racemic mixture yields non-chiral domains. As is most evident in Fig. 13 at $11.5\,\mathrm{mN\,m^{-1}}$, the predominant domain shape is like a bean with distinct cavities. As the monolayer is compressed, the domains grow and display their repulsive nature (arising from their oriented dipoles) by deforming themselves to fill all available space and transforming into polygons. At the surface pressures between 11 and $15\,\mathrm{mN\,m^{-1}}$, there happens a shape instability resulting in 'cutting' the domain along intrinsic chiral paths as shown in Fig. 13 at $14\,\mathrm{mN\,m^{-1}}$ (data not shown). This phase transition is attributed to the presence of the fluorescence probe, because no such effect is seen by Brewster angle microscopy [84]. In addition, the phase transition is completely suppressed at higher compression rates, suggesting a kinetic rather than a thermodynamic origin.

Monolayers of cerebroside used in this study do not form the LC domains in the monolayer. As the result, FM shows the liquid-expanded image (Fig. 13A and B). As mentioned in Section 2, cerebrosides are molecular species whose the hydrophobic parts are too bulky to be closely packed together compared with their occupied area of the polar head group. As the result, a cavity is formed among the hydrocarbon parts of LLC-2 because of the molecular structure. The white patterns in the FM image are the evidence of such LE domains independent on surface pressure (Fig. 13A).
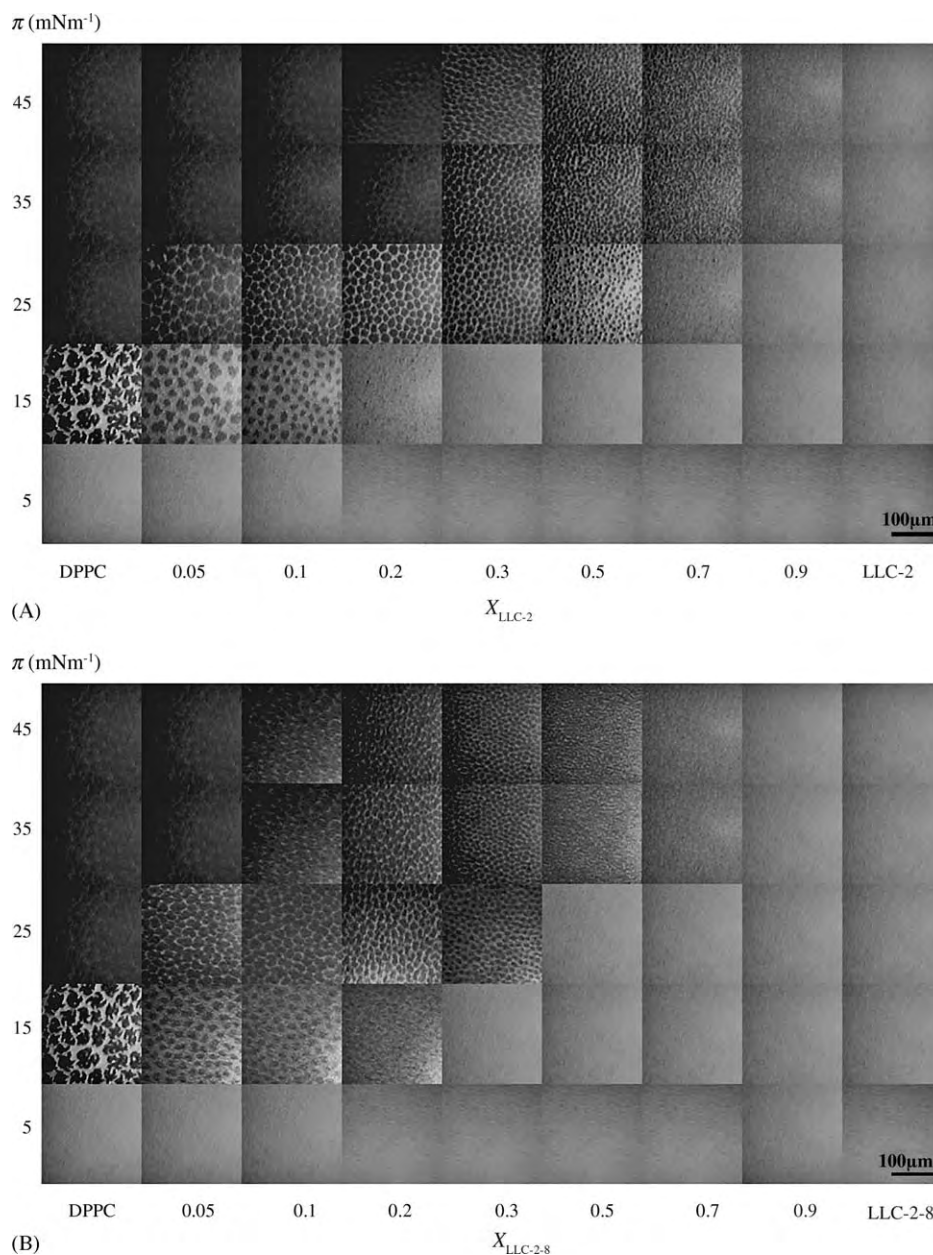
Fig. 13. Fluorescence micrographs of cerebroside/DPPC (two-component) monolayer as a function of $X_{cerebroside}$ observed at the compression rate of $1.0 \times 10^{-1} \, nm^2 \, molecule^{-1} \, min^{-1}$ at 298.2 K on 0.15 M NaCl. Numerical number shows mole fraction of cereborside. (A) LLC-2/DPPC; (B) LLC-2-8/DPPC, where the monolayer contained 1 mol% of fluorescent probe. The number in these images indicates the surface pressure (mN m^{-1}). Scale bar represents 100 μm.

Next, the mole fraction dependence of the transition pressure is observed on the FM images of the two-component system of LLC-2/DPPC in Fig. 13A for $X_{cerebroside} = 0.05$–0.7. At low surface pressures ($\pi < \pi^{eq}$), cerebroside/DPPC systems of the two-component monolayer were uniformly fluoresced, showing apparently homogeneous liquid-expanded (LE) phase without liquid-condensed (LC) phase of dark domains. Increasing the surface pressure, LC domains appear at $X_{cerebroside} = 0.05$–0.2. In each case, the LE/LC coexistence region is observed and transition pressure (π^{eq}) is higher than that of pure DPPC (Fig. 13A and B). This suggests that the observed dark domains in these figures would represent a con-

densed DPPC-enriched phase. With increasing the surface pressure, the conformational change of the polar head groups in the two-component monolayer is to facilitate the formation of the small LC domains of DPPC. The fluorescence images also supported the evidence of miscibility. Similarly the size of LC domains became smaller with the addition of LLC-2-8 in Fig. 13B, indicating the prevention of large domains by the mixing of LLC-2-8 into DPPC. For $X_{LLC-2-8} = 0.9$ the domains were too small to be visible as LLC-2-8. The sizes of LC domains were much smaller, compared with LLC-2/DPPC system, suggesting that the miscibility of LLC-2-8 to DPPC was easier than that of LLC-2. In morphology,

the pure compound LLC-2-8 behaves like as LE film or the molecular species. This proves that the terminal methyl group contributes much to packing of molecules at the surface.

The images of LLC-2-10, -12, -15 did not show the black domains, which suggested that these cerebrosides form tiny LC domains compared with normal LC domain.

To visualize the LC domains in FM image, much attention was paid to the experimental conditions such as temperature, subphase, compression speed, and spreading solvent. At first, temperature was decreased down to 283.2 K. Secondly, subsolution was changed concerning the concentration and pH (that is, 1, 2, 5 M NaCl, 2 M NaCl + pH 2 and 2 M NaCl + pH 12). Thirdly, compression rate was made slow in order to create the LC domain gradually at 5.2×10^{-3} nm^2 molecule^{-1} min^{-1} of compression rate. Finally, spreading solvent was changed to toluene/methanol (2:1) instead of chloroform/methanol (2:1). As the result, the LC domains could be observed for LLC-2-15 and -12 without changing the π–A isotherm profile. However, the domains were not so clear image like that of DPPC and appeared as gray domains. Here, the images were not shown, because they looked like homogeneous LE. This is one of the reasons why hydrophobic part of the terminal methyl group (*iso* and *anti-iso*) makes unfocused gray LC domain. The part of the terminal methyl group effects the π–A isotherm [86,87] profile and the branched chains affect the morphology [88]. Consequently, the LC domains could not exclude the fluorescence probe completely.

4. Conclusion

The cerebrosides (LLC-2, LLC-2-1, LLC-2-8, LLC-2-10, LLC-2-12, and LLC-2-15) derived from *L. laevigata* can be spread as a stable monolayer on 0.15 M NaCl solution at 298.2 K together with phospholipid (DPPC). The Demchak and Fort model was applied to analyze the surface potential of cerebrosides. Using the calculated saccharide polar head group, it became clear that the hydrophobic tail groups strongly influence the surface potential. The new findings were that LLC-2 showed LE film and that four components (LLC-2-8, -10, -12, and -15) have the first order LE/LC phase transition in the π–A isotherms at 298.2 K. The apparent molar quantity changes (Δs^{γ}, Δh^{γ}, and Δu^{γ}) on the phase transition on 0.15 M at 298.2 K were calculated. The apparent molar quantity changes depended on the chain length combination, which was based on the cohesive force of hydrocarbon chain in cerebrosides. The values of the apparent molar quantity changes on the phase transition for cerebrosides were almost the same as that of the tetradecanoic acid. This comes from the steric hindrance of the hydrophobic part packing by the terminal *iso*-type structure.

Comparing monolayer behaviors of the molecular species LLC-2 and the pure compound LLC-2-8 with that of DPPC, both binary systems of LLC-2/DPPC and LLC-2-8/DPPC were investigated. The miscibility was supported by the change of the transition pressure (π^{eq}) and the collapse pressure (π^{c}). The π–A and ΔV–A isotherms of cerebrosides/DPPC mixtures show that the two components are miscible in the monolayer state over the whole ranges of cerebroside mole fraction and of surface pressure investigated. From the A_m–$X_{cerebroside}$ and ΔV_m–$X_{cerebroside}$ plots, partial molecular surface area (PMA) and apparent partial molecular surface potential (APSP) were determined at different surface pressures. The PMA changes with the mole fraction were extensively discussed for the miscible system. On the other hand, the APSP changed depending upon the surface pressure for LLC-2/and LLC-2-8/DPPC systems. The two-dimensional phase diagram and the Joos equation allowed calculation of the interaction parameter (ξ) and interaction energy ($-\Delta\varepsilon$) between cerebrosides (LLC-2 and LLC-2-8) and DPPC for miscible binary systems. The one type of phase diagram was obtained: the positive azeotropic (cerebrosides/DPPC). The interaction of LLC-2-8 and DPPC is a bit stronger than that of LLC-2 and DPPC. The fluorescence images also supported the miscibility. Fluorescence microscopy for two-component cerebrosides/DPPC monolayers on 0.15 M NaCl solution showed that cerebrosides dissolved the LC domains of DPPC monolayer upon compression. These phenomena indicated that the miscibility of two-component system is influenced by an extent of packing of hydrophobic group.

Although the pure compound LLC-2-8 has LE/LC transition pressure, LLC-2-8 behaves just like LE film or the molecular species in the morphology. This proves that the terminal methyl structure (*iso* or *anti-iso*) contributes much to molecular packing. It can be supposed that the molecular species of LLC-2 at their surfaces regulate such fundamental biological processes as growth, differentiation, and motility as the functions of animal cells by the competition and/or the cooperation of multi-components (such as LLC-2-1, -8, -10, -12, and -15). It also suggested that the molecular species in biological systems play an important role in controlling the fluidity and the packing of the biomembrane. Furthermore, the terminal methyl group plays an important role in controlling the fluidity and the packing of the biomembrane.

References

[1] N. Kojima, S. Hakomori, J. Biol. Chem. 264 (1989) 20159.
[2] M. Tiemeyer, Y. Yasuda, R.L. Schnaars, J. Biol. Chem. 264 (1989) 1671.
[3] N. Kojima, N. Kurosawa, T. Nishi, N. Hanai, S. Tsuji, J. Biol. Chem. 269 (1994) 30451.

[4] T. Mutoh, A. Tokuda, T. Miyadai, M. Hamaguchi, N. Fujiki, Proc. Natl. Acad. Sci. U.S.A. 92 (1995) 5087.

[5] K. Simons, D. Toomre, Nat. Rev. 1 (2000) 31.

[6] T. Farooqui, T. Franklin, D.K. Pearl, A.J. Yates, J. Neurochem. 68 (1997) 2348.

[7] S. Tagami, J. Inokuchi, K. Kabayama, H. Yoshimura, F. Kitamura, S. Uemura, C. Ogawa, A. Ishii, M. Saito, Y. Ohtsuka, S. Sakaue, Y. Igarashi, J. Biol. Chem. 277 (2002) 3085.

[8] H. Nojiri, H. Manya, H. Isono, H. Yamana, S. Nojima, FEBS Lett. 453 (1999) 140.

[9] Y. Suzuki, T. Nakao, T. Ito, N. Watanabe, Y. Toda, X. Guiyun, T. Suzuki, T. Kobayashi, Y. Kimura, A. Yamada, K. Sugawara, H. Nishimura, F. Kitame, K. Nakamura, E. Deya, M. Kiosi, A. Hasegawa, Virology 189 (1992) 121.

[10] B. Alberts, Molecular Biology of the Cell, 3rd ed., Garland Publishing Inc., New York, 1994.

[11] B. Maggio, Prog. Biophys. Mol. Biol. 62 (1994) 55.

[12] R.A. Demel, Y. London, W.S.M. Geurts Van Kessel, F.G.A. Vossenberg, L.L.M. Van Deenen, Biochim. Biophys. Acta 311 (1973) 507.

[13] R. Koynava, M. Caffrey, Biochim. Biophys. Acta 1255 (1995) 213.

[14] K. Simons, E. Ikonen, Nature 387 (1997) 569.

[15] R.E. Brown, J. Cell Sci. 111 (1998) 1.

[16] E. Kobayashi, K. Motoki, T. Natori, T. Uchida, H. Fukushima, Y. Koezuka, Biol. Pharm. Bull. 19 (1996) 350.

[17] M. Morita, K. Motoki, K. Akimoto, T. Natori, T. Sakai, E. Sawa, K. Yamaji, Y. Koezuka, E. Kobayashi, H. Fukushima, J. Med. Chem. 38 (1995) 2176.

[18] W. Stoffel, A. Bosio, Curr. Opin. Neurobiol. 7 (1997) 654.

[19] S. Figueroa-Perez, R.R. Schmidt, Carbohydrate Res. 328 (2000) 95.

[20] T. Tencomnao, R.K. Yu, D. Kapitonov, Biochim. Biophys. Acta 1517 (2001) 416.

[21] C.E.M. Hollak, E.P.M. Corssmit, J.M.F.G. Aerts, E. Endert, H.P. Sauerwein, J.A. Romijn, M.H.J. van Oers, Am. J. Med. 103 (1997) 185.

[22] T. Murakami, T. Shimizu, K. Taguchi, Tetrahedron 56 (2000) 533.

[23] S. Kawatake, K. Nakamura, M. Inagaki, R. Higuchi, Chem. Pharm. Bull. 50 (2002) 1091.

[24] M. Inagaki, K. Nakamura, S. Kawatake, R. Higuchi, Eur. J. Org. Chem. (2003) 325.

[25] J.M. Lassaletta, R.R. Schmidt, Tetrahedron Lett. 36 (1995) 4209.

[26] H. Löfgren, I. Pascher, Chem. Phys. Lipids 20 (1977) 273.

[27] J.M. Smaby, V.S. Kulkarni, M. Momsen, R.E. Brown, Biophys. J. 70 (1996) 868.

[28] C.R. Flach, R. Mendelsohn, M.E. Rerek, D.J. Moore, J. Phys. Chem. B 104 (2000) 2159.

[29] D.C. Carrer, B. Maggio, Biochim. Biophys. Acta 1514 (2001) 87.

[30] M. Saito, H. Kitamura, K. Sugiyama, Biochim. Biophys. Acta 1511 (2001) 271.

[31] K. Arao, M. Inagaki, T. Miyamoto, R. Higuchi, Chem. Pharm. Bull. 52 (2004) 1140.

[32] S. Kawatake, M. Inagaki, T. Miyamoto, R. Isobe, R. Higuchi, Eur. J. Org. Chem. (1999) 765.

[33] K. Yamada, R. Matsubara, M. Kaneko, T. Miyamoto, R. Higuchi, Chem. Pharm. Bull. 49 (2001) 447.

[34] M. Inagaki, R. Isobe, R. Higuchi, Eur. J. Org. Chem. (1999) 771.

[35] F. Cateni, J. Zilic, G. Falsone, G. Scialino, E. Ban, Bioorg. Med. Chem. Lett. 13 (2003) 4345.

[36] N. Takakuwa, K. Saito, M. Ohnishi, Y. Oda, Biores. Technol. 96 (2005) 1089.

[37] B. Maggio, Chem. Phys. Lipids 132 (2004) 209.

[38] F. Bordi, F. De Luca, C. Cametti, A. Naglieri, R. Misasi, M. Sorice, Colloids Surf. B 13 (1999) 135.

[39] K. Matsuura, H. Kitakouji, R. Oda, Y. Morimoto, H. Asano, H. Ishida, M. Kiso, K. Kitajima, K. Kobayashi, Langmuir 18 (2002) 6940.

[40] C.M. Rosetti, R.G. Oliveira, B. Maggio, Langmuir 19 (2003) 377.

[41] M. Diociaiuti, I. Ruspantini, C. Giordani, F. Bordi, P. Chistolini, Biophys. J. 86 (2004) 321.

[42] C. Yuan, J. Furlong, P. Burgos, L.J. Johnston, Biophys. J. 82 (2002) 2526.

[43] C. Yuan, L.J. Johnston, Biophys. J. 81 (2001) 1059.

[44] S. Yokoyama, T. Takeda, T. Tsunoda, Y. Ohta, T. Imura, M. Abe, Colloids Surf. B 27 (2002) 141.

[45] S. Yokoyama, T. Takeda, M. Abe, Colloids Surf. B 27 (2002) 181.

[46] (a) R. Ledeen, J. Neurosci. Res. 12 (1984) 147;
(b) Y.A. Hannum, R.M. Bell, Science 243 (1989) 500.

[47] S. Hakomori, J. Biol. Chem. 265 (1990) 18713.

[48] J.M. Harouse, S. Bhat, S.L. Spitalnik, M. Laughlin, K. Stefano, D.H. Silberberg, F. Gonzales-Scarano, Science 253 (1991) 320.

[49] H. Nakahara, S. Nakamura, K. Nakamura, M. Inagaki, M. Aso, R. Higuchi, O. Shibata, Colloid Surf. B 42 (2005) 157.

[50] S. Nakamura, O. Shibata, K. Nakamura, M. Inagaki, R. Higuchi, Stud. Surf. Sci. Catal. 132 (2001) 447.

[51] H. Nakahara, S. Nakamura, K. Nakamura, M. Inagaki, M. Aso, R. Higuchi, O. Shibata, Colloid Surf. B 42 (2005) 175.

[52] E. Okuyama, M. Yamazaki, Chem. Pharm. Bull. 31 (1983) 2209.

[53] K. Aida, M. Kinoshita, M. Tanji, T. Sugawara, M. Tamura, J. Ono, N. Ueno, M. Ohnishi, J. Oleo. Sci. 54 (2005) 45.

[54] B. Maggio, F.A. Cumar, R. Caputto, Biochem. J. 171 (1978) 559.

[55] B. Maggio, F.A. Cumar, R. Caputto, Biochem. J. 175 (1978) 1113.

[56] D.S. Johnston, E. Coppard, D. Chapman, Biochim. Biophys. Acta 815 (1985) 325.

[57] J.P. Slotte, A.L. Östman, E.R. Kumar, R. Bittman, Biochemistry 32 (1993) 7886.

[58] A.H. Berglund, P. Norberg, M.F. Quartacci, R. Nilsson, C. Liljenberg, Physiol. Plant. 109 (2000) 117.

[59] Z. Moldovan, E. Jover, J.M. Bayona, Anal. Chim. Acta 465 (2002) 359.

[60] S. Sugiyama, M. Honda, T. Komori, Liebigs Ann. Chem. (1990) 1063.

[61] M. Inagaki, R. Isobe, Y. Kawano, T. Miyamoto, T. Komori, R. Higuchi, Eur. J. Org. Chem. (1998) 129.

[62] T. Maruta, T. Saito, M. Inagaki, O. Shibata, R. Higuchi, Chem. Pharm. Bull., in press.

[63] T. Hiranita, S. Nakamura, M. Kawachi, H.M. Courrier, T.F. Vandamme, M.P. Krafft, O. Shibata, J. Colloid Interface Sci. 265 (2003) 83.

[64] H. Nakahara, S. Nakamura, H. Kawasaki, O. Shibata, Colloids Surf. B 41 (2005) 67.

[65] R.J. Demchak, T. Fort Jr., J. Colloid Interface Sci. 46 (1974) 191.

[66] J.T. Davies, E.K. Rideal, Interfacial Phenomena, 2nd ed., Academic Press, New York and London, 1963, p. 71.

[67] V. Vogel, D. Möbius, Thin Solid Films 159 (1988) 73.

[68] D.M. Taylor, O.N.J. Oliveira, H.J. Morgan, J. Colloid Interface Sci. 139 (1990) 508.

[69] J.G. Petrov, E.E. Polymeropoulos, H. Möhwald, J. Phys. Chem. A 100 (1996) 9860.

[70] M.K. Bernett, N.L. Jarvis, W.A. Zisman, J. Phys. Chem. 68 (1964) 3520.

[71] C.P. Smyth, Dielectric Behaviour, Structure, McGraw-Hill, New York, 1955.

[72] M.K. Bernett, W.A. Zisman, J. Phys. Chem. 67 (1963) 1534.

[73] J. Marsden, J.H. Schulman, Trans. Faraday Soc. 34 (1938) 748.

[74] D.O. Shah, J.H. Schulman, J. Lipid Res. 8 (1967) 215.

[75] M. Kodama, O. Shibata, S. Nakamura, S. Lee, G. Sugihara, Colloids Surf. B 33 (2004) 211.

[76] C.A. Helm, H. Möhwald, K. Kjaer, J. Als-Niesen, Biophys. J. 52 (1987) 381.

[77] O. Albrecht, H. Gruler, E. Sackman, J. Phys. (France) 39 (1978) 301.

[78] V.M. Kagner, H. Möhwald, P. Dutta, Rev. Mod. Phys. 71 (1999) 779.

[79] Y.K. Levine, Prog. Surf. Sci. 3 (1973) 279.
[80] K. Motomura, T. Yano, M. Ikematsu, H. Matuo, R. Matuura, J. Colloid Interface Sci. 69 (1979) 209.
[81] M. Rusdi, Y. Moroi, S. Nakamura, O. Shibata, Y. Abe, T. Takahashi, J. Colloid Interface Sci. 243 (2001) 370.
[82] P. Joos, R.A. Demel, Biochem. Biophys. Acta 183 (1969) 447.
[83] C.W. McConlogue, T.K. Vanderlick, Langmuir 13 (1997) 7158.
[84] C.W. McConlogue, T.K. Vanderlick, Langmuir 14 (1998) 6556.
[85] C.W. McConlogue, D. Malamud, T.K. Vanderlick, Biochim. Biophys. Acta 1372 (1998) 124.
[86] D.K. Rice, D.A. Cadenhead, R.N.A.H. Lewis, R.N. McElhaney, Biochemistry 26 (1987) 3205.
[87] D.M. Balthasart, D.A. Cadenhead, R.N.A.H. Lewis, R.N. McElhaney, Langmuir 4 (1988) 180.
[88] D. Vollhardt, G. Emrich, S. Siegel, R. Rudert, Langmuir 18 (2002) 6571.